NEXRES 3 (2026) 101132

Contents lists available at ScienceDirect

Next Research

journal homepage: www.elsevier.com/locate/nexres

Optimization of production process of agro-based activated carbon for sustainable cooling systems

Rasheed B. Ayoola [a], Olusegun M. Ilori [a,*], Sikiru A. Amidu [b], Maryam T. Buhari [a], Moruf O. Yusuf [c], Alex O. Edeoja [d], Jacob S. Ibrahim [d]

[a] School of Architecture, Built Environment, Computing, and Engineering, Birmingham City University, Birmingham, United Kingdom
[b] Seplat Energy Producing Nigeria Unlimited, 1 Lekki Expressway, Victoria Island, Lagos, Nigeria
[c] Department of Civil Engineering, University of Hafr Al Batin, Hafar Al Batin, Saudi Arabia
[d] Department of Mechanical Engineering, Joseph Sarwuan Tarka University, Makurdi, Benue, Nigeria

ARTICLE INFO

Keywords:
Raphia nut endocarp-derived activated carbon (RNEAC)
Agro-waste valorization
Chemical activation
Hybrid optimization techniques
Solid adsorption refrigerators (SARs)
Machine learning

ABSTRACT

This study investigates the experimental production and multi-objective optimization of the production process of microporous activated carbon (AC) derived from Raphia nut endocarp (RNE) for solid adsorption refrigerators (SARs) and related systems. Using phosphoric acid (H_3PO_4) and calcium chloride ($CaCl_2$) as activating agents, a comprehensive optimization technique integrating genetic algorithms (GA), Pareto optimality (PO), min-max normalization (MMN), and machine learning (ML) was applied to determine the optimal RNE-derived AC (RNEAC) properties, including surface area, carbon yield, and ash content. Linear regression was used as the ML algorithm to analyze the relationship between the production variables of the RNEAC. The experimental design varied parameters such as carbonization temperature, residence time, activating agent concentration, and impregnation ratio, to statistically evaluate their impacts. Results revealed that temperature and residence time significantly influence ash content, while impregnation ratio, temperature, and residence time optimize surface area. Similarly, carbon yield was affected by temperature, residence time, and impregnation ratio. The optimized RNEAC exhibits properties that include a high surface area, low ash content, and a promising methanol adsorption capacity, highlighting its suitability for application in SARs. This study will contribute to achieving a greener environment and the development of high-efficiency and sustainable adsorption cooling technologies for rural communities by valorizing agricultural wastes and turning them into excellent low-cost adsorbents for the next generation of SARs.

1. Introduction

The growing demand for sustainable and environmentally friendly cooling technologies is directly tied to the escalating impacts of global warming. Agriculture alone contributes 30 % of global anthropogenic greenhouse gas (GHG) emissions, primarily methane and nitrous oxide from land-based sources [1–4]. Developing countries disproportionately contribute to these emissions due to inefficient farming practices, inadequate product storage facilities, and poor waste management. In sub-Saharan Africa, postharvest losses range between 15 % and 50 %, resulting in an estimated annual loss of $4 billion due to inadequate storage facilities [5]. The resulting wastes from surplus crops significantly add to landfill emissions and environmental degradation [6–9]. Cold chain infrastructure is critical for rural and off-grid areas to mitigate these challenges and ensure product quality and economic stability [10,11]. Solid adsorption refrigerators (SARs), which rely on activated carbon (AC) as an adsorbent, and on efficient heat exchangers for effective heat and mass transfer [12], offer a sustainable solution for off-grid cooling. SARs maintain stable low temperatures, helping to reduce spoilage of perishable crops by 25 % to 35 % and supporting food security, particularly in regions with limited electricity access, such as remote northern parts of Nigeria [13–19]. While cold rooms are used in many rural areas for vaccine and crop preservation, frequent project failures are common due to unreliable power supply. A viable alternative is to use locally sourced materials for adsorbent production, which is a critical component in a solid adsorption regeration (SAR) system. These systems require minimal electricity, involve straightforward activation methods, and support modular and decentralized manufacturing. The RNEAC production, in particular, can provide an

* Corresponding author.
E-mail addresses: Olusegun.ilori@bcu.ac.uk (O.M. Ilori), SAmidu@seplatenergy.com (S.A. Amidu).

https://doi.org/10.1016/j.nexres.2025.101132
Received 13 January 2025; Received in revised form 25 June 2025; Accepted 24 November 2025
Available online 25 November 2025

Nomenclature

W_{ASC}	Weight Ash Content
N_{ASC}	Normalized Ash Content
W_{SA}	Weight Surface Area
N_{SA}	Normalized Surface Area
N_{CY}	Normalized Carbon Yield
X	Original data point
$X_{normalised}$	Normalized dataset
X_{min}	Datapoint with a minimum value
X_{max}	Data point with the maximum value
f_m	Objective function
CD_{im}	Crowding distance
R_i	Ranking of Non-dominated Pareto front
R_j	Ranking of Non-dominated Pareto front
AC	Activated carbon
ANOVA	Analysis of Variance
CCD	Central Composite Design
CI	Confidence Interval
DOE	Design of Experiments
GA	Genetic Algorithm
GHG	Greenhouse Gas
GP	Genetic programming
HFC	Hydrofluorocarbon
HVACR	Heating, ventilation, air-conditioner, and refrigeration
IDE	Integrated Development Environment
MAE	Mean Absolute Error
MOGA	Multi-Objective Genetic Algorithm
MOO	Multi-objective optimization
MSE	Mean Square Error
NSGA - II	Non-dominated Sorting Genetic Algorithm II
PI	Prediction Interval
RNE	Raphia nut endocarp
RNEAC	Raphia nut endocarp-derived activated carbon
RSA	Response Surface Analysis
RSM	Response Surface Methodology
SAR/SARs	Solid adsorption refrigerator (refrigeration)/ refrigerators
SE	Standard Error
SEM	Scanning Electron Microscopy
STD	Standard Deviation
VOC	Volatile Organic Materials

economical, scalable, and environmentally friendly solution tailored to the needs of rural areas in developing countries. Its integration into SARs could enhance food and vaccine preservation, create employment, and reduce seasonal waste buildup, making it a transformative strategy for underserved communities.

SARs use AC, which can be sustainably sourced from agricultural byproducts, such as the Raphia nut endocarp (RNE). RNE is abundant in West Africa and is a cost-effective and renewable resource that can be used sustainably. Studies have shown that it contains a carbon content of over 70 %, making it suitable for high-performance adsorbents [20,21]. When chemically activated, RNE achieves a surface area of up to 1200 m^2/g, enhancing adsorption efficiency [22–24]. Chemical agents like phosphoric acid (H_3PO_4) and calcium chloride ($CaCl_2$) lower carbonization temperatures by up to 20 %, reduce tar formation and optimize pore development, which is essential for producing high-quality AC [25,26]. Utilizing RNE in AC production supports circular economic principles by converting agricultural waste into a value-added product and reducing environmental burdens associated with improper waste disposal [7]. This approach can significantly contribute to regional economic growth by using underutilized agro-waste resources.

Despite its potential, Nigeria's lack of locally developed AC production technologies limits the adoption of SARs for critical applications, including food and vaccine storage. Producing AC from indigenous resources such as RNE could address this gap, providing a sustainable cooling solution that aligns with the country's environmental and economic priorities [10,11]. AC's exceptional properties, such as a high adsorption capacity of 0.5 to 1.5 g/g refrigerant and a pore volume exceeding 0.8 cm^3/g, make it indispensable for application in SARs [27,28]. These characteristics enhance the operation efficiency of SARs, enabling applications in solar-powered refrigeration system, where energy savings of up to 30 % have been reported [29,30]. RNE-derived AC (RNEAC) also addresses regional waste management challenges, with studies estimating that 40 % of agricultural byproducts in West Africa remain unutilized [7,8]. This makes RNE an economically viable precursor for localized AC production. Also, studies have confirmed that agro-waste AC often meets and exceeds the performance of commercially available adsorbents, making it a sustainable alternative for application in SARs in rural and off-grid regions [31,26]. In the context of sustainability, RNEAC is preferable because it can be developed from agricultural residue, supporting efficient material usage and mitigating environmental impact. Compared to commonly used synthetic alternatives, such as silica gel and Zeolite [15], RNEAC is cheaper to produce, adaptable to suit specific applications by varying activation time and temperature, and can be locally produced, to promote economic and environmental sustainability [17,32,33].

Chemical activation techniques are critical for enhancing AC properties. Agents such as H_3PO_4 and $ZnCl_2$ can produce AC with porosities ranging from 300 to 2000 m^2/g, which exceed commercial standards [34,23]. The performance of AC can be significantly influenced by its pore structure. Pores in AC can be classified into three categories based on their diameter. Micropores (<2 μm), mesopores (2–50 μm), and macropores (>50 μm), as defined by IUPAC (International Union of Pure and Applied Chemistry). These three categories contribute to adsorption efficiency, as found by Yakout and Sharaf El-Deen [24] and Reza et al. [23], who emphasized that micropores provide a high surface area for adsorbate intake, mesopores ensure molecular transport and prevent channel blockage, while serving as pillars for other categories.

Pore size distribution (PSD) can be obtained via several methods, such as Nitrogen (N_2) Physisorption [35,36] and Scanning Electron Microscopy (SEM) [37,38]. Applying the N_2 physisorption model requires stringent precautions, because N_2 adsorption to micropores is often diffusionally limited, leading to an incorrect value of PSD [36,39]. Various studies have used image analysis software on SEM images to quantify particle pore size and distribution as well as classify surface morphology. One popular method for such analysis is the use of ImageJ, an open-source image software. For instance, Maheshwaran et al. [40] investigated water retention potential of coconut shell (CS) aggregates and how they could be reduced using this method. The SEM image of the precursor was analyzed using ImageJ for microstructural analysis of pore properties, including the number of pores and the minimum, maximum and mean pore areas. Their analysis indicated a minimum pore area of 2 μm^2, a 75–85 % threshold efficiency, and 8-bit and RGB image types, yielding comparable pore area and percentage values. Agboola et al. [41] synthesized AC from Olive seeds for dye removal. The authors performed quantitative pore and interpore spacing analyses using ImageJ on SEM images to characterize the pore network accurately. Also, Chilev et al. [37] present a quantitative approach to characterizing porous solid material based on SEM and ImageJ analysis. The study highlighted the effectiveness of SEM analysis to characterize porous solid materials, including pore size distribution (PSD), surface area, and pore volume, thereby eliminating the need for supplementary analytical approaches, such as adsorption-based methodologies.

The efficiency of AC also depends on its moisture and ash content. Moisture levels, typically between 3 % and 10 %, ensure optimal adsorption while minimizing carbon dilution [42]. Ash content, typically ranging from 2 % to 10 %, influences the structural stability and catalytic properties of AC, making it a critical production parameter [43]. Hybrid activation methods, which combine chemical and physical processes, have further enhanced the cost-effectiveness and sustainability in AC production, offering production cost savings of up to 15 % compared to conventional methods [44,45]. By leveraging resources such as RNE and advanced activation methods, AC production can play a transformative role in supporting the development of sustainable and high-efficiency SAR, reducing environmental impacts and creating economic opportunities for local communities [7,46,26]. Therefore, the sustainable cooling potential of RNEAC can be summarized as twofold – its production from abundant agro-waste using cost-effective activation methods ensures low-cost, scalable production of adsorbent. At the same time, its high adsorption capacity enhances SAR performance, enabling energy-efficient cooling solutions suitable for off-grid deployment.

Producing AC with excellent adsorption properties for SARs involves balancing carbon yield, ash content, and surface area, making it a complex multi-objective optimization problem. Advanced hybrid optimization techniques such as genetic algorithms (GA), Pareto optimality (PO), and min-max normalization (MMN) are increasingly used to streamline this process [47,48]. These methods enable researchers to navigate high-dimensional parameter spaces, ensuring optimal trade-offs without compromising crucial performance metrics. For instance, the use of GA for AC production has been shown to improve adsorption efficiency by 10–20 % through iterative solution evolution, while NSGA-II variants enable precise Pareto-optimal balancing across multiple objectives [30,49]. Elham Kabiri and Negin Maftouni [50] optimized a trade centre's energy efficiency using NSGA-II genetic algorithms and environmentally friendly materials and achieved a 52.3 % energy reduction, 37.3 % cooling load decrease, and 167.67 tons of CO2 savings. PO ensures no parameter improvement compromises another, fostering balanced decision-making [44]. Meanwhile, MMN standardizes variables across scales, thereby minimizing bias and ensuring the equitable treatment of competing objectives [51]. Research using response surface methodology (RSM) has demonstrated its efficacy in identifying optimal parameters for producing AC with enhanced adsorption properties from agricultural residues such as corn cobs [52].

Although traditional multi-objective optimization methods, such as dynamic programming, offer precise results, they are computationally intensive and time-consuming. Modern heuristic techniques, including simulated annealing and artificial neural networks, provide significant efficiency improvements but require rigorous parameter tuning [53]. Hybrid models integrating GA with PO and MMN have demonstrated remarkable versatility, addressing constraints across various applications. For instance, multigene geometric programming has improved adsorption rates by 15 %, while min-max robustness models have significantly enhanced system reliability [54–56]. These advanced methods highlighted the potential for producing AC that will improve SAR efficiency and its sustainability by optimizing the production process parameters.

The application of machine learning methods to optimize AC production parameters has significantly contributed to the adaptation of this technology for specific applications. These methods facilitate the efficient synthesis of application-specific adsorbents for various uses. Liao et al. [57] demonstrated the effectiveness of ANN in predicting AC yield and surface area from various biomass feedstocks. Their findings showed that the model achieved R^2 above 0.9, implying accurate prediction. Similarly, Chang and Lee [58] utilized Random Forest and Support Vector Machine (SVM) to predict the adsorption capacity of biochar-activated carbon synthesized from waste wood. The models were optimized, and they compared favourably with the ANN.

Despite significant advancements in AC production, challenges remain in achieving scalable and cost-effective methods. Hybrid optimization techniques, such as GA, PO, and MMN, have effectively addressed multi-objective trade-offs, including ash content, carbon yield, and surface area. However, these methods often face difficulties in fully resolving non-linear relationships among variables in complex systems. This study tackles these challenges by integrating advanced statistics, machine learning, and optimization methods into a comprehensive framework for producing application-specific RNEAC tailored to applications in SARs. Linear regression was used solely as a predictive model for response features based on experimental factors. Subsequently, GA/PO was optimized based on the regression outcome. By incorporating linear regression, normalization models, and error analysis tools, the approach ensures precise control over production conditions and performance metrics, thereby enhancing optimization outcomes and enabling the development of AC with optimized properties for efficient SAR systems.

Crucial experimental parameters such as carbonization temperature, residence time, activating agent concentration, and impregnation ratio are systematically optimized to produce high-quality RNEAC. This tailored adsorbent enhances the efficiency of SARs, particularly with natural refrigerants like ammonia, CO_2, and methanol. The fact that these natural refrigerants have a negligible global warming potential (GWP) and do not deplete the ozone layer, makes them environmentally superior to synthetic alternatives, such as HFCs. The proposed optimization framework can enhance SAR performance, reduce GHG emissions, and promote the valorization of agricultural waste. These outcomes align with global sustainability goals, offering significant environmental and economic benefits, especially for rural and off-grid communities. By leveraging RNE as a renewable precursor for AC, this research advances waste management solutions and contributes to the development of off-grid cooling technologies. By integrating sustainable materials with advanced optimization techniques, SARs can be positioned as a viable solution for addressing pressing environmental and economic challenges in underserved regions.

2. Materials and methods

2.1. Sample collection, preparation and characterisation

The experimental data is obtained from the test setup described in Ayoola et al. [25]. Details of the use of acid (H_3PO_4) and salt ($CaCl_2$) as activating agents in the preparation of RNEAC were discussed, and the authors comprehensively describe the experimental setup, sample collection, preparation, and characterization of RNEAC. Chemical activation of high-carbon agro-waste materials (as shown in Fig. 1), such as RNE, has proven especially effective, as it optimizes microporous structures and contributes to environmental sustainability [31,26].

2.2. Chemical activation pathway of RNE in rneac production

The activation process of RNE involved impregnating the precursor with activating agents ($CaCl_2$ and H_3PO_4) for 24 h. Each activator plays a distinct role in pore development during this chemical treatment. At the impregnation phase, the phosphoric acid (H_3PO_4) assists in dehydration and cross-linking reactions within the precursor's lignocellulosic structure. This chemical interaction facilitates a steady structure of carbon, which prevents tar formation during pyrolysis. As the material is heated post-impregnation, H_3PO_4 supports the formation of a polyphosphate matrix, which is typically washed off after treatment to leave behind a well-developed micro and mesoporous structure. On the other hand, $CaCl_2$ facilitates pore formation by extracting volatile organic materials and water during carbonization. This salt penetrates the precursor's internal matrix, causing disruption and expanding it to create pore networks. The residual calcium compounds are washed with distilled water to further enhance the carbon porosity. The choice of $CaCl_2$ and H_3PO_4 as activating agents can be justified because they have been proven effective in improving the pore sizes and surface structure of

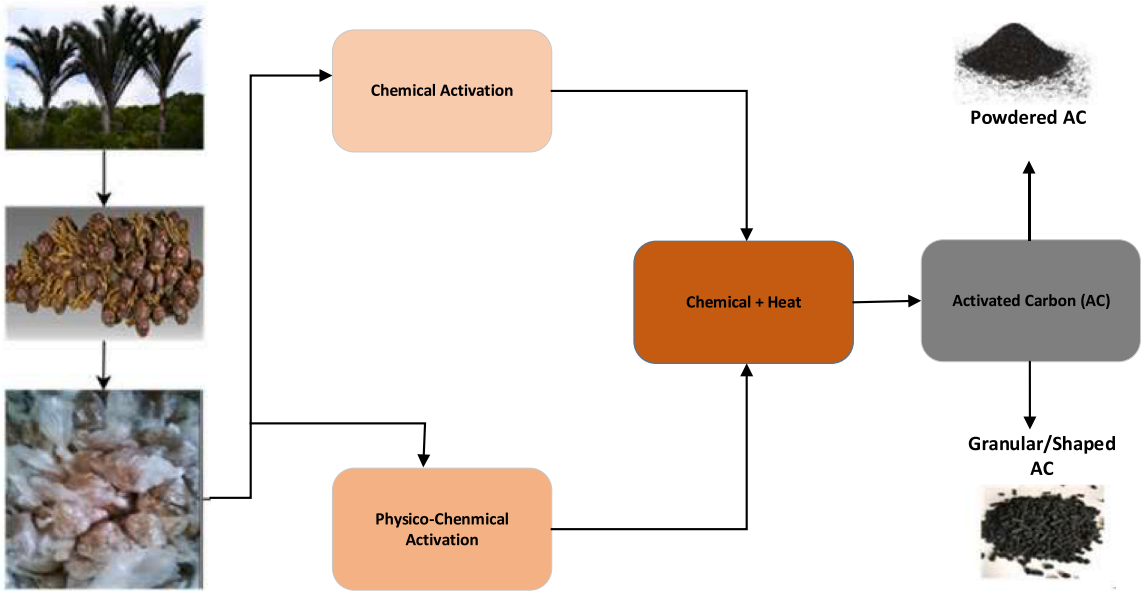

Fig. 1. Chemical Activation for Activated Carbon.

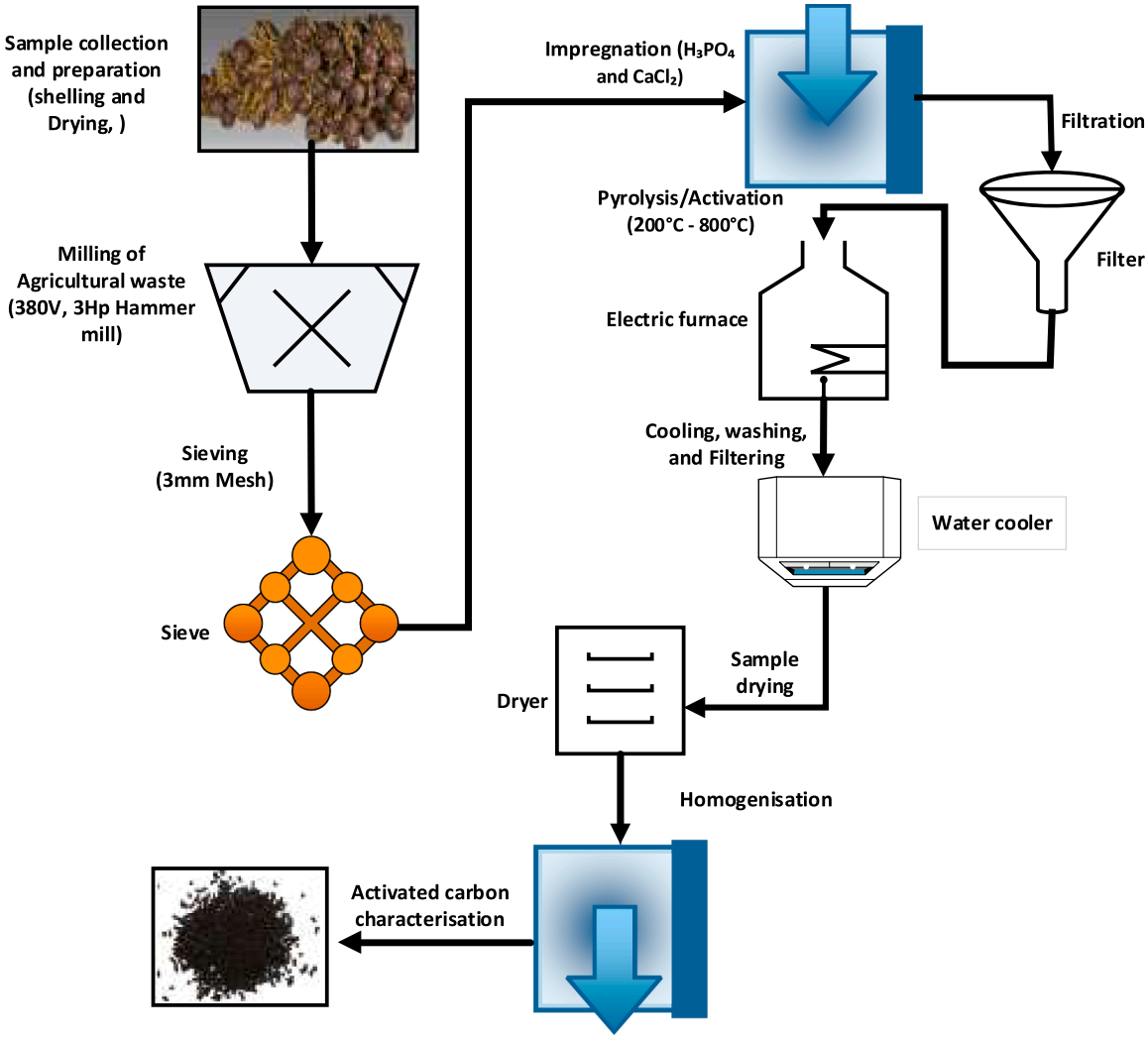

Fig. 2. Flowchart for synthesizing chemically activated Raphia-nut-based activated carbon.

lignocellulosic precursors converted to AC [59,60]. $CaCl_2$, a neutral salt, promotes the development of micropores through a mild dehydration mechanism, whereas H_3PO_4 aids in forming mesoporous structures and positively impacts surface functionalities [61,62].

Studies on activation methods indicate that chemical activation, like phosphoric acid, is particularly effective for applications like solvent recovery, while physical activation is more commonly used for water treatment purposes [63,64]. Chemical activation was chosen because this study focuses on RNEAC for application in SARs. This study employs a concentration gradient protocol for sample impregnation, following the method described by Caturla et al. [65]. For brevity, Fig. 2 illustrates the flow process for preparing, characterizing, and optimizing RNEAC production. Critical factors, such as the activating agent concentration, carbonization temperature, residence time, and impregnation ratio, were selected based on their economic viability and environmental impact, as guided by the literature data. H_3PO_4 and $CaCl_2$, known for their oxidation and dehydration properties [66], were used to evaluate the effect of acid concentration on the three performance metrics. Their synergistic application in comparative investigations facilitates a thorough assessment of activation mechanisms conducive to adsorption or catalytic functionalities. Fig. 3 shows the application of RNEAC in a SAR setup. Further details about the test rig are not repeated here as they have been published elsewhere. Table 1 shows the chemical properties of the RNEAC, while Table 2 shows equations (1 – 5) used for the AC evaluation.

2.2. overview of dataset attributes

The data was collected through factorial experimental design, which involves varying two or more factors in parallel to observe their impact on a response variable. All numeric values have been carefully measured and recorded, to ensure accuracy and reliability for optimization purposes. The dataset utilized to optimize RNEAC comprises four crucial input parameters and three overarching responses, as described in Table 3.

2.3. Optimization of production parameters

A hybrid optimization approach was employed to identify optimal production parameters using GA, PO, ML and advanced statistics (including linear regression models, optimization-model, error analysis, and standard deviation of the optimization score). In optimizing AC production using agro-based precursors (e.g., RNE) and chemical activation methods, various process variables such as activation temperature, residence time, activator concentration, and yield characteristics frequently exhibit non-uniform scales and units. Min-max normalization is considered relevant due to the multidimensional features involved in the production of RNEAC. It standardizes all input parameters to a consistent range (typically from 0 to 1), ensuring that no individual parameter disproportionately influences the optimization process due to its numerical magnitude.

Table 1
The Chemical Composition of Raphia Palm Seed.

Element	Composition (%)
Carbon	39
Oxygen	4.21
Hydrogen	0.172
Sulphur	0.03
Nitrogen	3.703

(Source: [13]).

Table 2
Equations for activated carbon evaluation (Equations 1–5).

Carbon properties	Governing equation	Legend	Author
MoistureContent (%)	$\left(\frac{W_1 - W_2}{W_1} \times 100\right)$ (Eq. 1)	W_1 =initial weight of the known quantity of activated carbon. W_2 = Final weight after heating for 1 hour at 105°C	[8]
Ash content (%)	$\frac{Ash\ weight(g)}{Over\ dry\ weight(g)} \times 100$ (Eq. 2)		[8,67]
Bulk density $B_d\left(\frac{g}{mL}\right)$	$W_s = W - W_c$ $\frac{W_s}{V_s}$ (Eq. 3)	W_c = weight of the empty cylinder. W_s = weight of the sample. V_s = Volume occupied by the packed sample. W = weight of the crucible plus weight of the sample	[[8, 67]
CarbonYield (%)	$\frac{W_f}{W_{ca}} \times 100$ (Eq. 4)	$W_{ca}(g)$ = The dried weight of precursor. W_f = Dry weight of RNEAC	[68]
Surface Area (m^2/g)	$\frac{6(m^2/g)}{B_d P_d}$ (Eq. 5)	B_d = particle bulk density P_d = the particle diameter	[8,67]

2.3.1. Genetic algorithms (GA)

GA evolve diverse solution sets within a population through selection, crossover, and mutation cycles, effectively addressing conflicting objectives [47]. In this study, GA is employed to identify near-optimal solutions. The NSGA-II algorithm enables multi-objective optimization by identifying non-dominated solutions, facilitating the exploration of trade-offs and achieving balanced outcomes across the study's objectives [69]. Equation 1 presents the general form of the multi-objective function, summarising the GA computation process.

a) Sort all "I" solutions in a Pareto front in ascending order of f_m and compute.

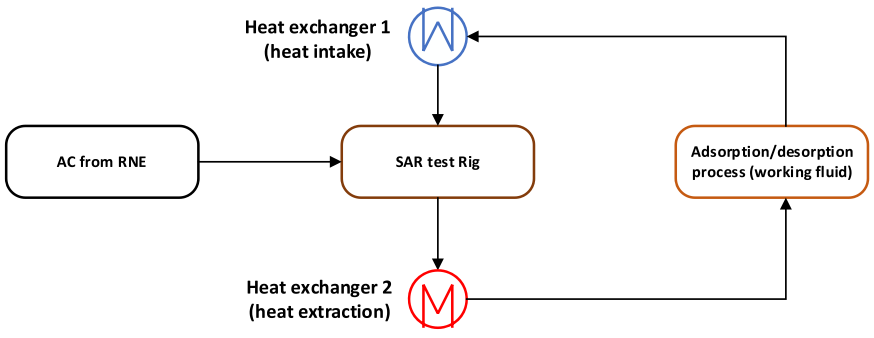

Fig. 3. Flow process of RNEAC application in SARs.

Table 3
Input and output parameters for process optimization.

Factor			Response		
Input parameters	Input Level/ range	Input steps	Output parameters	Obtained value	Targeted value
Carbonization Temperature	200 – 600 °C	200 °C	Ash contents (%)	1 - 24.5 %,	2.50 %
Impregnation ratio	1 – 4	1	Carbon yield (%)	64.6 - 73.7 %	75 %
Concentration of the Activating agent	25 - 100 %	25 %	Surface area (m^2/g)	1400 – 2200 (m^2/g)	1400 (m^2/g)
Soaking/ residence time	30 - 120 min	30 min	-	-	-

$$CD_{im} = \frac{f_m(x_{i+1}) - f_m(x_{i-1})}{f_m(x_{max}) - f_m(x_{min})}, \mathrm{i} = 2, \ldots\ldots\ldots, (l-1) \tag{6}$$

Where CD_{im} and f_m are Crowding distance and Objective function, respectively.

a) Repeat step 1 for each objective and find the crowding distance of solution I.

$$CD_i = \sum_{m-1}^{M} CD_{im} \tag{7}$$

Given two solutions i and j with the following condition, solution i is preferred to solution j if:

$$R_i < R_j or \ \left(R_i = R_j \ and \ CD_i > CD_j\right) \tag{8}$$

R_i – Ranking of Non dominated Pareto front $i = 1$
R_j – Ranking of Non dominated Pareto front $j = 2 \ldots N_{ranking}$

2.3.2. Pareto optimality

In multi-objective optimization problems, the goal is to achieve the optimal decision-making outcome. PO seeks to optimize multiple competing objectives simultaneously, ensuring that improving one does not worsen another [54]. The mathematical formulation for MOO using PO is given in Equation 4 [56].

$$\begin{aligned} f1;\mathrm{opt} &= \min f1(x) \ \text{seekstominimize} \ f1(x). \\ f2;\mathrm{opt} &= \min f2(x) \ \text{seekstominimize} \ f2(x). \\ fn;\mathrm{opt} &= \min fn(x) \ \text{seekstominimize} \ fn(x). \end{aligned} \tag{9}$$

The objective functions $f1$ (x), $f2$ (x)…, fn (x) are independently optimized in a bid to seek simultaneous optimization of all objectives. In this context, x^* represents a Pareto optimal solution where a feasible solution x exists, as illustrated in Equation 5.

$$\begin{aligned} &f1(x) \le f1(x^*), f2(x) \le f2(x^*), \ldots, fn(x) \ge fn(x^*) \ (\text{forminimizationobjectives}). \\ &f1(x) \ge f1(x^*), f2(x) \ge f2(x^*), \ldots, fn(x) \le fn(x^*) \ (\text{formaximizationobjectives}). \end{aligned} \tag{10}$$

2.3.3. Min-Max Normalisation

Although PO can identify the Pareto frontier solutions, inconsistencies may still arise due to differences in objective scales, complicating decision-making that requires precise trade-offs (Ehrgott et al., 2014). Min-max normalization is a suitable scaling technique for mitigating these inconsistencies by reducing the impact of uneven data distributions. While various normalization techniques exist, their effectiveness depends on the statistical characteristics of the dataset. This study employs the min-max approach due to its ability to handle outliers effectively, either by addition or removal as needed, ensuring a consistent and uniformly scaled solution set [70]. This method adjusts data by subtracting the minimum value and then dividing by the range of each variable (i.e., the difference between maximum and minimum limits), as shown in Eq. (6).

$$x_{normalised} = \frac{x - x_{min}}{x_{max} - x_{min}} \tag{11}$$

Where, $x, x_{normalise}, x_{min},$ *and* x_{max} are the original data point, normalized dataset, data point with minimum value and data point with maximum value, respectively.

Each response variable from the dataset for the two activating agents (H_3PO_4 and $CaCl_2$) was normalized based on the Min-Max normalization criteria as follows:

$$Ash\_Content\_Normalised = \frac{min(Ash\_Content)}{Ash\_Content} \tag{12}$$

$$Surface\_Area\_Normalised = \frac{Surface\_Area}{\max\ (Surface\_Area)} \tag{13}$$

$$Carbon\_Yield\_Normalised = \frac{Carbon\_yield}{Max(Carbon\_Yield)} \tag{14}$$

2.3.4. Optimization model

Improving and standardizing existing production processes through optimization is a continuous process, as current methods still require adaptation to emerging conditions. Therefore, the summation of the normalized values indicates that the optimization goal is to maximize the combined effect of these normalized parameters. The optimization score (S_{opt}) is defined as:

$$Sopt = \sum_{i=1}^{3} w_i x_i \tag{15}$$

Where X_i *represents* each of the normalized variables and $w_i$are the weight of the dependent variables while the sum goes from $I = 1$ to 3

2.3.5. Machine learning algorithm and advanced statistics

Machine learning models exhibit varying performance depending on internal and external factors influencing their application process, making it essential to evaluate multiple models to identify the most suitable one for a given problem. A linear regression algorithm based on input variables is applied to predict the RNEAC preparation process outputs (ash content, surface area, and carbon yield). The model is tested on two experimental datasets (H_3PO_4 and $CaCl_2$ activations) applied to the same precursor under identical conditions. The process parameters are optimized using MMN and GA, and cross-validation is employed to assess the model's stability. This is implemented in Visual Studio Code (VS Code 1.92.2) using Python 3.11 and relevant data-processing libraries such as deap, matplotlib, pandas, and numpy.

2.3.6. Linear regression model

Eq. (16) represents the quadratic model applied to experimental data from RNEAC production to examine the relationships between the

predictor variables (temperature, concentration, impregnation ratio, and residence time) and responses (Ash content, surface area and carbon yield).

$$Y = \beta_0 + \sum_{i=1}^{4} \beta_i X_i + \sum_{i=1}^{4} \beta_{ii} X_i^2 + \sum_{1=1}^{4} \beta_{ij} X_i X_j + \epsilon \quad (16)$$

Where Y is the response variable, X_i are the input parameters, β_0 β_i β_{ii} β_{ij} are coefficients, and ϵ Is the error term.

2.3.7. Error analysis

The accuracy of the ML is measured using error metrics, including Mean Absolute Error (MAE) and Mean Square Error (MSE), which provide the error between the actual and predicted values. Similarly, R^2 quantifies the proportion of variance explained by the LR model employed in this study. MAE and MSE are computed using:

$$MAE = \frac{1}{n} \sum_{i=1}^{n} |y_i - \hat{y}_i| \quad (17)$$

$$MSE = \frac{1}{n} \sum_{i=1}^{n} (y_1 - \hat{y}_1)^2 \quad (18)$$

y_i is the actual value, $\hat{y}_i$ is the normalized/predicted value, and n is the number of data points

The coefficient of Performance R^2 is represented by Eq. (19)

$$R^2 = 1 - \frac{\sum_{i=n}^{1} (y_i - \hat{y}_i)^2}{\sum_{i=n}^{1} (y_i - \bar{y})^2} \quad (19)$$

$\bar{y}$ is the mean of the actual values

Eq. (20) illustrates the residual ε_i between the ith original value y_i and normalized value $\hat{y}_i$ is expressed as

$$\varepsilon_1 = y_i - \hat{y}_i \quad (20)$$

2.3.8. Standard deviation of optimization score

The standard deviation of the optimization score is calculated as:

$$\sigma\ (Optimisation\ Score) = \sqrt{1/n \sum_{i=1}^{n} (X_i - \mu)^2} \quad (21)$$

Where:

X_i is the $i-$ th Optimization Score,

μ is the mean of the Optimization Scores, and n is the number of optimization scores.

The variance of the Optimization Score is the square of the standard deviation, given as

$$\text{Var}(\ \text{OptimizationScore}\ ) = \sigma(optimisationScore)^2 \quad (22a)$$

2.4. Evaluation of experimental results

The study employs multi-objective weighted sum optimization (MOWSO) and machine learning techniques, including NSGA-II and regression analysis, to evaluate the performance of GA, PO, and MMN in optimizing RNEAC production parameters. These methods focus on achieving the study's objectives of minimizing ash content while maximizing surface area and carbon yield. PO solutions are generated and analyzed for the two activators used, providing insight into the effectiveness of the optimization technique. The optimal production conditions identified through hybrid optimization were validated by reproducing AC samples under these conditions. The properties of these samples were compared with initial experimental results to confirm the reliability and robustness of the optimization approach. Results are compared with data from the literature, such as the surface structure from SEM micrographs. It is essential to determine the specific values of factors that affect every quality of the developed adsorbent [71]. On this basis, we adopt the response optimization results through the Design of Experiments (DOE). The best solutions obtained from this experiment were ranked using composite desirability scores, with the first ranking representing superior quality.

3. Results and discussion

3.1. SEM-Based surface morphology analysis

The surface morphology of H_3PO_4-RNEAC was examined using scanning electron microscopy (SEM) at a magnification of 713x and 502x and different scale bars of 50 μm and 100 μm, as depicted in Fig. 4 (a & b). The micrographs show a heterogeneous surface structure with a network of irregularly formed pores and voids, indicative of the formation of a porous architecture critical for adsorption applications. The pore dimensions observed fall within the micrometre scale (~10–50 μm), suggesting macroporosity. This irregularity enhances the specific surface area, reported to range from 800 to 1200 m^2/g in similar studies by Khalil et al. [72], which is crucial for adsorption applications such as SAR systems. The distinct voids and irregular surface morphology support the material's potential for adsorptive phenomena, partially compensating for the lack of Brunauer–Emmett–Teller (BET) surface area assessments. The visual evidence substantiates the effective activation and morphological development of the carbonaceous adsorbent. SEM images reported by Khalil et al. [72], Martinez et al. [73], and Yahya et al. [21] underscore the influence of biomass precursor type on AC surface morphology, complementing RNEAC's analysis. Different biomass-AC exhibits distinct surface morphology with specific effects on accessibility and adsorption efficiency. Olive pit-derived AC exhibits a flatter surface, reducing pore accessibility and adsorption efficiency. Walnut shell and coconut shell ACs exhibit spherical pores averaging 4–6 μm, while oil palm fruit bunches and bamboo stems have irregular pores exceeding 10 μm [21]. These differences can be attributed to variations in the lignin and cellulose content across precursors, which in turn influence the carbonization process and the final morphology. H_3PO_4 activation (Fig. 5b) forms a well-structured matrix dominated by mesopores (~2–50 nm) and micropores (<2 nm), achieving a specific surface area of 1400–1600 m^2/g [74]. This distribution is optimal for SAR systems that adsorb refrigerants, such as methanol.

The surface area of RNEAC was evaluated using semi-quantitative methods identified as 'SEM + ImageJ' techniques, as shown in Fig. 4 (c & d). These figures illustrate feature segmentation and a binary image showing pores filled with red particles as the feature of interest. In this method, SEM images were analyzed using ImageJ to evaluate pore sizes. The calibration of the SEM image, thresholding, and particle analysis yielded 1378 unique features. The average pore area was 52.12 μm^2 (Perimeter = 18.72 μm), with a total surface coverage of approximately 21.07 %, indicating a relatively high porosity. These results suggest that the adsorbent possesses a moderately dense and evenly distributed pore network, which may influence its adsorbate affinity or fluid transport properties. The quantitative insights gained from SEM analysis through ImageJ are essential for evaluating RNEAC suitability in SARs. As indicated in Fig. 4e, the log-scaled histogram illustrates that most pores fall within the range of 1 to 10 μm^2, with an exponential decline in frequency for larger sizes. This indicates a tightly arranged microporous structure where smaller pores are predominantly present. Table 4 shows the results of the 'SEM + ImageJ' analysis for important parameters. Fig. 5 (a-d) illustrates the application process and the result of the 'SEM + ImageJ' for $CaCl_2$-RNEAC at a magnification of 1.5 kx, which indicates a low pore network within the adsorbent matrix. $CaCl_2$ activation generates larger pores (>10 μm) with a lower density, ideal for rapid diffusion in air filtration applications. This result is consistent with previous findings ([21]) where $ZnCl_2$-activated samples exhibit extensive microporosity, accounting for >60 % of the pore volume. Also, KOH and K_2CO_3 activations yield intermediate pore sizes, thereby balancing the adsorption capacities for volatile organic compounds (VOCs) and

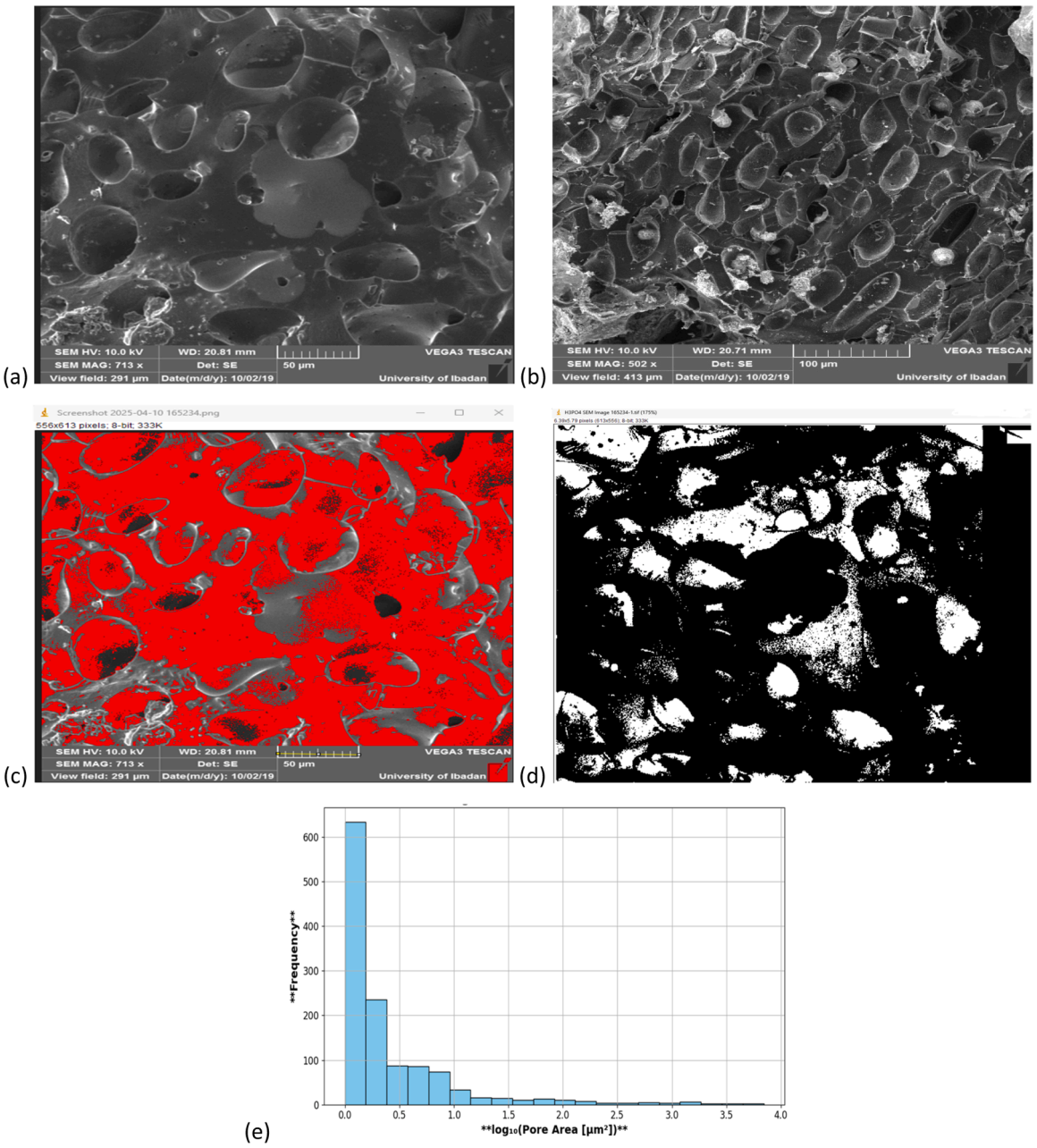

Fig. 4. SEM + ImageJ analysis of pore size and distribution for H_3PO_4-RNEAC: (a) SEM Image (713 x), (b) SEM Image (502x), (c) Feature segmentation stage on ImageJ analysis for 713x maginification (d) Binary image showing pores in white (e) Log-scaled pore size distribution analysis in SEM + ImageJ.

hydrocarbons.

The observed differences in pore size and distribution across samples (cf. Figs. 4& 5) suggest that activating agents can be tailored to optimize ACs for specific applications. For instance, H_3PO_4 activation is ideal for SAR systems that require high refrigerant adsorption capacities, while $CaCl_2$ activation is better suited for VOC removal and catalytic processes due to their enhanced mesoporosity. From a sustainability perspective, using biomass as a precursor ensures environmental benefits, while tailored activation methods maximize efficiency, making biomass-derived ACs a promising option for sustainable and environmentally friendly cooling solutions.

3.2. Optimization from scenario rankings

Table 5 presents the optimized values for various properties and post-treatment features of RNEAC. A comparative analysis was conducted to identify the most favorable scenarios by maximizing surface area and carbon yield while minimizing ash content, as detailed in Appendices 1–2. Appendix 1 explicitly highlights the results of the PO analysis performed in MATLAB using MOGA [53].

This normalization ensured comparability across variables measured on different scales. Equal weights were assigned to the three response variables (ash content, carbon yield, and surface area), and an aggregate score for each scenario was calculated using a weighted sum as described in Eq. (22). The results, presented in Fig. 7, illustrate the effectiveness of this approach in reflecting balanced preferences across the response variables.

$$Composite\ score = \sum_{i=1}^{3} (W_i\ X\ N_i) \tag{22}$$

Where:

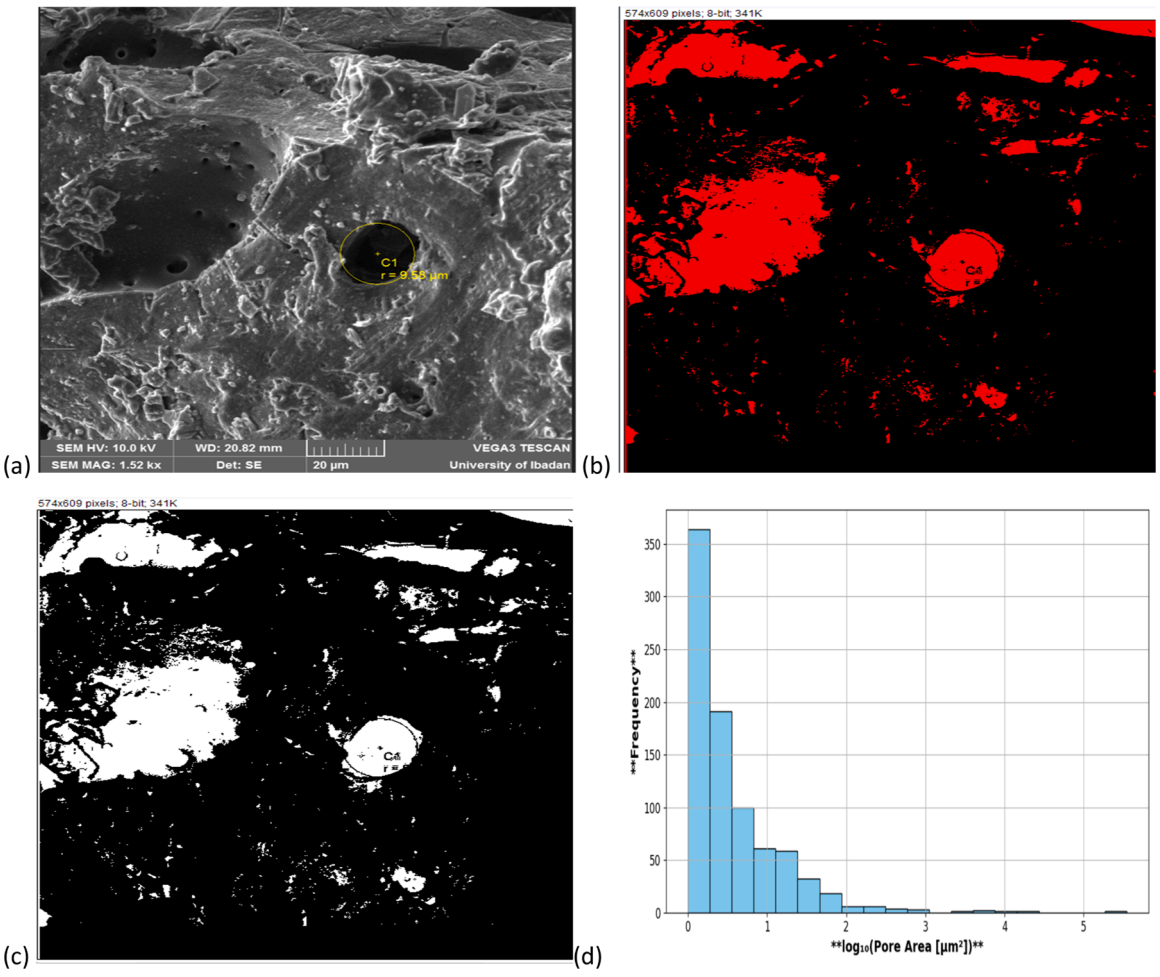

Fig. 5. SEM + ImageJ analysis of pore size and distribution for $CaCl_2$-RNEAC (a) SEM Image (1.52kX), (b) Feature segmentation stage on ImageJ, (c) Binary image showing pores (white), and (d) Log-scaled pore size distribution analysis in SEM + ImageJ.

Table 4
Summary – Results of SEM + ImageJ analysis of RNEAC.

Slice	Count	Total Area	Average Size	1%Area	Mean	Perim.	Circ.	Feret	MinFeret
SEM_H3PO4_ 165,234.png	1378	71,822	52.12	21.073	255	18.721	0.873	5.077	3.043

$W_1 = W_{ASC,}$ $W_2 = W_{SA,}$ and $W_3 = W_{CY}$. $N_1 = N_{ASC,}$ $N_2 = N_{SA,}$ and $N_3 = N_{CY}$

Each scenario is ranked in ascending order based on its composite score, with lower scores indicating better options according to the criteria. Scenarios 1 and 26, identified as having the lowest scores, represent the optimized values for RNEAC production (see Appendix 2).

Table 5
Optimized scenarios for RNEAC production with composite scores.

	Ranked Scenario 1	Ranked Scenario 2
Scenarios	26	1
Impregnation ratio (-)	2.416	2.2972
Temperature (°C)	400.38	400.2
Residence Time (mins)	111	109.72
Concentration (%)	75.737	75.392
Ash Content (%)	1.0573	1.0447
Carbon Yield (%)	73.211	73.15
Surface Area (m^2/g)	1401.7	1402.3
Composite Score	0.000269	0.000387

These scenarios (highlighted in Fig. 6) best meet the criteria of high carbon yield, high surface area, and low ash content.

In Fig. 7 (a & b), bar plots of normalized scores for each response are shown to compare the normalized values of the dependent variables under optimal conditions. In Fig. 7a, a clear trade-off can be observed between carbon yield and ash content for $CaCl_2$-RNEAC, where minimizing ash content (approximately 0.05) results in a high normalized carbon yield score (about 0.9). However, this reduction in ash content has a relatively low impact on surface area. Conversely, for H_3PO_4-RNEAC (Fig. 7b), the trade-off between ash content and the other two responses, carbon yield and surface area, is more significant and consistent. This highlights the influence of activating agents on the optimum yield and surface area of AC.

Fig. 8 illustrates the Pareto-front of the three objectives using convergence and diversity metrics. Converged points represent normalized results, while divergent points indicate the distribution across the Pareto front. The scatter plot reveals scenarios where lower composite scores correspond to higher values for carbon yield and surface area [51]. The chart shows pronounced divergence compared to convergence, reflecting significant trade-offs among ash content, carbon yield, and surface area and highlighting a wide range of non-dominated

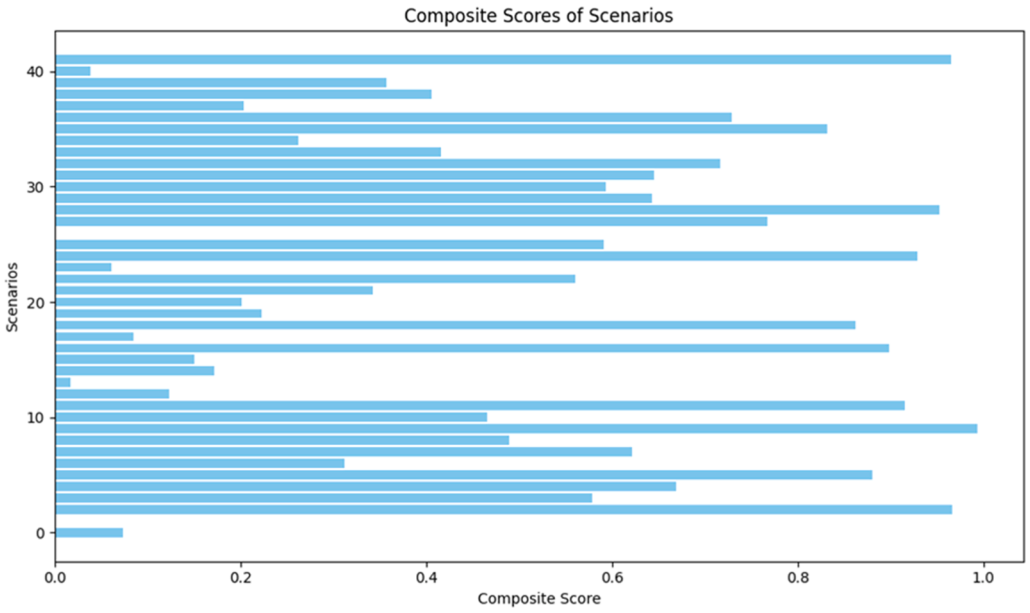

Fig. 6. Composite scores distribution across scenarios for RNEAC production.

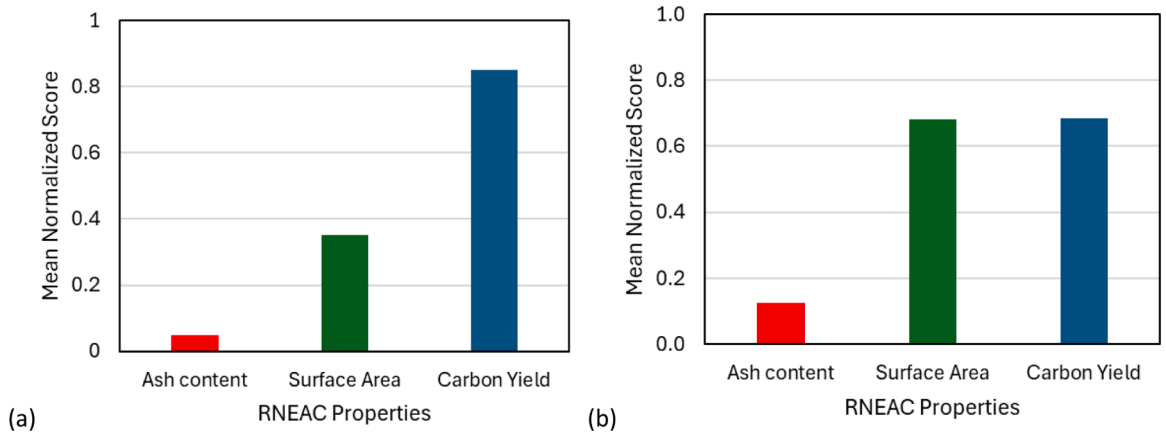

Fig. 7. Bar Plot of normalized scores for (a) $CaCl_2$, (b) H_3PO_4.

solutions. Optimizing for surface area and carbon yield tends to result in higher composite scores, as shown by the deep-coloured points in the Z-plane. Fig. 9 (a & b) further visualizes these trade-offs using a colour gradient to depict the interplay between the objectives. The plot balances carbon yield and surface area, with the colour bar illustrating the influence of ash content on each Pareto optimal solution.

Multiple trials were conducted to optimize the process parameters for producing RNEAC, necessitating an analysis of experimental uncertainty. Fig. 10 (a & b) shows the error bars for the two activators, illustrating the relationship between input parameters and optimization scores. While a few outliers are present, most temperature levels at 200 °C and 400 °C exhibit lower optimization scores compared to the 600 °C level in both cases.

3.2.1. *Response optimization*

The objective of optimizing the RNEAC production process is to minimize the ash content while maximizing surface area and carbon yield, adhering to recommendations in the literature for producing economically viable, high-quality AC [21]. Optimizing multiple objectives in parallel can be challenging due to conflicting goals. Therefore, Response Surface Analysis (RSA) from the Design of Experiments (DOE) is used to evaluate scenarios that generate response optimization values. This approach aggregates the performance of all objective functions into a unified benchmark, simplifying decision-making [75,53]. The optimization results yielded 17 optimal solutions for the three responses (Carbon yield, surface area, and ash content), as shown in Appendix 3. The goal and parameter settings (setting limits and targets) for response variables are shown in Table 6. Based on the equal weight assigned to all responses, any solutions can give factor values (elements) that affect the responses (quality) the most. However, the composite desirability of 0.710484 corresponds to the values most affected by every quality. The corresponding elements (factors) are 212.121 °C, 100 %, 120 min, and 4 g/g for Temperature, Concentration, Resident time, and impregnation Ratio, respectively.

As shown in Tables 7 and 8, the best fit indicates RNEAC's superior carbon yield as 74.11 % at optimal factors of 212.121 °C, 100 %, 120

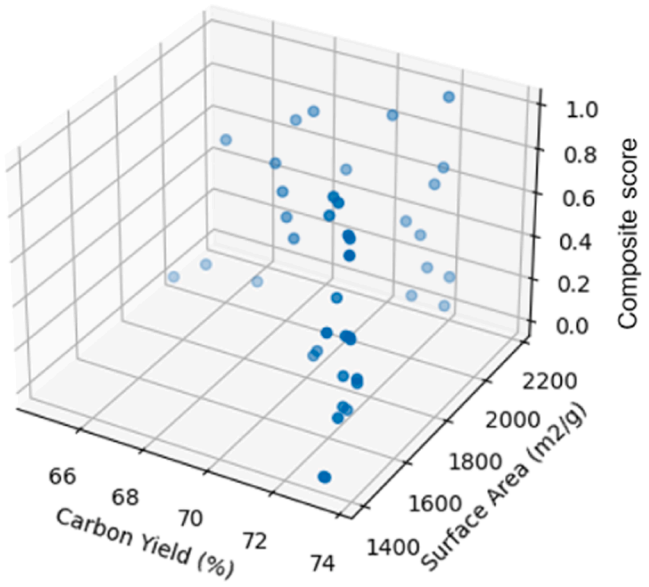

Fig. 8. Composite scores distribution across scenarios for RNEAC production.

min, and 4 g/g for temperature, concentration, resident time, and impregnation ratio, respectively. Other qualities, such as surface area and carbon yield corresponding to the optimal factors, are 1755 m^2/g and 12.46 %, respectively. The RNEAC exhibit an optimal surface area superior to that of a typical commercially available activated carbon, with a surface area ranging from 800–1000 m^2/g, as Wu et al. [76] reported. RNEAC result is also comparable with 1450 m^2/g reported by Sun & Webley [77] when evaluating the surface area of AC from corn cob precursor using K_2CO_3 as an activating agent. Table 8 shows the values of Fit, Standard error of fit (SE Fit), confidence interval (CI) and prediction interval (PI) for response variables. The carbon yield is expected to lie between 63.84 and 85.70 under the given optimal conditions with 95 % confidence (see Table 6). On the other hand, the 95 % confidence interval suggests that the true mean for carbon yield falls between 70.89 and 78.66.

3.3. *Effect of input variables*

The experiment data is presented in Fig. 11 (a & b). Using a central composite design (CCD) for the experimental design, the process variables for RNEAC preparation are distributed across various levels for each scenario. The plot of the optimization score versus temperature suggests that the optimization score is better at higher temperatures, indicating that lower temperatures are less effective in producing high

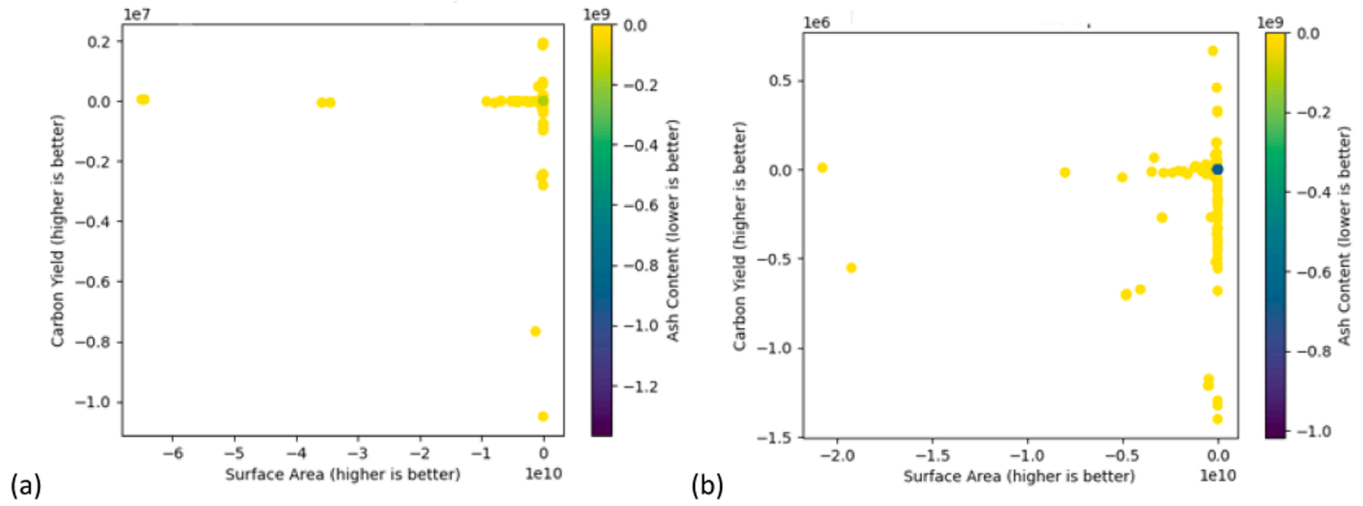

Fig. 9. Composite scores distribution across scenarios for RNEAC production (a) $CaCl_2$ (b) H_3PO_4.

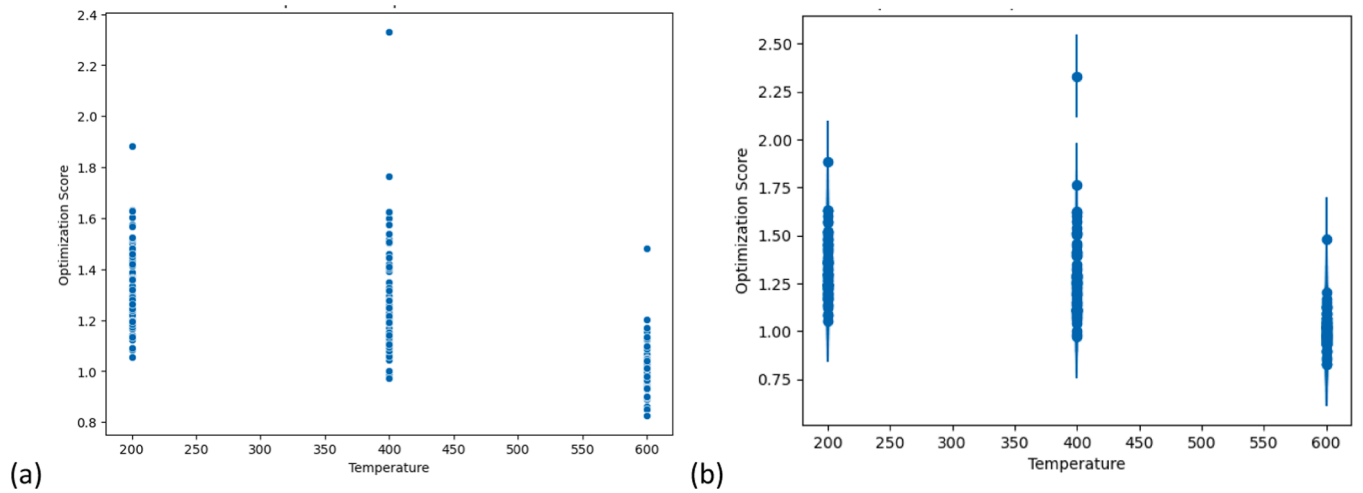

Fig. 10. Error bar for temperature against optimization score.

Table 6
Goal and parameter settings for the response variables.

Response	Goal	Lower Limit	Target	Upper Limit	Weight	Importance
Carbon Yield (%)	Maximum	55.48	82.10		1	1
Surface Area (m^2/g)	Maximum	387.80	4000.00		1	1
Ash Content (%)	Minimum		0.22	50.18	1	1

Table 7
Multiple response prediction.

Variable	Setting
Temperature (°C)	212.121
Concentration (%)	100
Resident Time (mins)	120
Impregnation Ratio (-)	4

Table 8
Fit, standard error of fit, confidence interval and prediction interval for response variables.

Response	Fit	SE Fit	95 % CI	95 % PI
Carbon Yield (%)	74.77	1.97	(70.89, 78.66)	(63.84, 85.70)
Surface Area (m^2/g)	1755	121	(1516, 1994)	(1084, 1426)
Ash Content (%)	12.46	3.76	(5.04, 19.88)	(−8.40, 33.32)

RNEAC yields. However, the scatter plots for the optimization score versus the other three process variables do not reveal clear trends, making it challenging to determine their impact on RNEAC yields. The experimental data suggest that identifying an optimized mix of input variables to maximize outputs while minimizing others is complex and time-consuming. The Kernel Density Estimate (KDE) plot of the optimization score shows that the median optimization score across experiments is approximately 96 %.

Fig. 12 illustrates the correlations between input variables and the optimization score. Insignificant correlations among the input variables confirm the absence of multicollinearity, which is critical for maintaining the statistical power of regression analyses. Temperature exhibits a relatively strong positive correlation (22e-16) with residence time, while concentration shows a negligible negative correlation with the impregnation ratio and residence time. Additionally, the heatmap of the correlation matrix (Fig. 12a) indicates a very weak positive correlation (5.4e-17) between residence time and concentration. A comparative evaluation of approaches for combining optimized preparation variables is essential. Moreover, the correlation matrix for $CaCl_2$ in Fig. 12b shows a null relationship between input variables, which may reflect the weak influence of the activating agent on the AC precursor.

Fig. 13 (a & b) presents the histogram plots showing the frequency distribution of residuals for the dependent variables associated with the two activating agents ($CaCl_2$ and H_3PO_4). The sinusoidal trendlines observed in the histograms confirm a non-linear relationship between the dependent and independent variables, justifying the use of models that can account for non-linearity. While this trend is evident in both datasets, the variable range is more evenly distributed in the $CaCl_2$ group (Fig. 13a) compared to the H_3PO_4 group (Fig. 13b). A logarithmic transformation was applied to address the overfitting observed in the initial residuals, regularising the model and ensuring a more robust prediction of response variables for the RNEAC.

Table 9 presents the ML-optimized process parameters for the RNEAC. Unlike the Pareto front analysis, which highlights trade-offs between multiple objectives, ML-based optimization reduces uncertainty, offering a more definitive solution.

3.4. Error analysis result

Metrics such as MAE, MSE, cross-validation, STD, and variance of the optimization score were evaluated to evaluate model performance using Eqs. (17) - 22. MAE and MSE were calculated between each dependent variable's normalized and actual values. Table 10 shows that the MAE and MSE values for each dependent variable are statistically significant compared to the Pareto front values normalized for max-min optimization, indicating that the problem formulation and algorithm design align well with the dataset. Additionally, the low mean cross-validation error (0.0381 ± 0.00814) and STD of the optimization score (0.22) suggest strong regression model performance. The actual optimization scores, 2.20 and 2.33 for H_3PO_4 and $CaCl_2$, respectively, exceed the STD of the optimization score, further confirming the model's reliability.

Fig. 14 (a-c) illustrate the trade-offs between the three objectives of RNEAC process optimization: maximizing carbon yield and surface area while minimizing ash content. Fig. 14a represents the Pareto Optimal Front (POF) for the objective functions "carbon yield" maximization and "ash content" minimization, where the concavity in the plot depicts the trade-off within the solution space. Similarly, Fig. 14b shows the POF for maximizing surface area and minimizing ash content. Fig. 14c shows the POF for maximizing carbon yield and surface area. A non-dominated solution for all three objectives can be observed as the POF in the plots [78]. Suboptimal regions outside the POF represent outcomes that fail to satisfy the objectives. These results underscore the need to apply PO to manage the competing objectives addressed in this study.

3.5. Analysis of experimental outcome

Analysis of the experimental data confirms the optimization. Fig. 15a illustrates the impact of residence time on the ash content at specific temperatures, revealing a dependency of RNEAC's ash content on activation time and carbonization temperature. At 400 °C, ash content consistently decreases with increasing residence time. However, at 200 °C and 600 °C, ash content initially declines up to a residence time of 2 min before increasing, with the highest ash content observed at 200 °C. This dynamic suggests that at temperatures above the optimum, useful AC transforms into ash, while below the optimum, the small yield of AC converts to ash as residence time increases. The decline in ash content at 400 °C with increasing residence time aligns with the optimization outcomes derived from Pareto-NDSGA II-Min-Max Normalization (cf. Appendix 2). These findings are further supported by Analysis of Variance (ANOVA) described in Appendices 4–6, confirming the statistical significance of temperature and its interaction with residence time in influencing ash content. This underscores the critical role of residence time and carbonization temperature in adjusting ash content, thereby validating the optimization results and reinforcing their robustness across various analytical methods. Fig. 15b illustrates the impact of residence time on ash content across different concentrations of H_3PO_4.

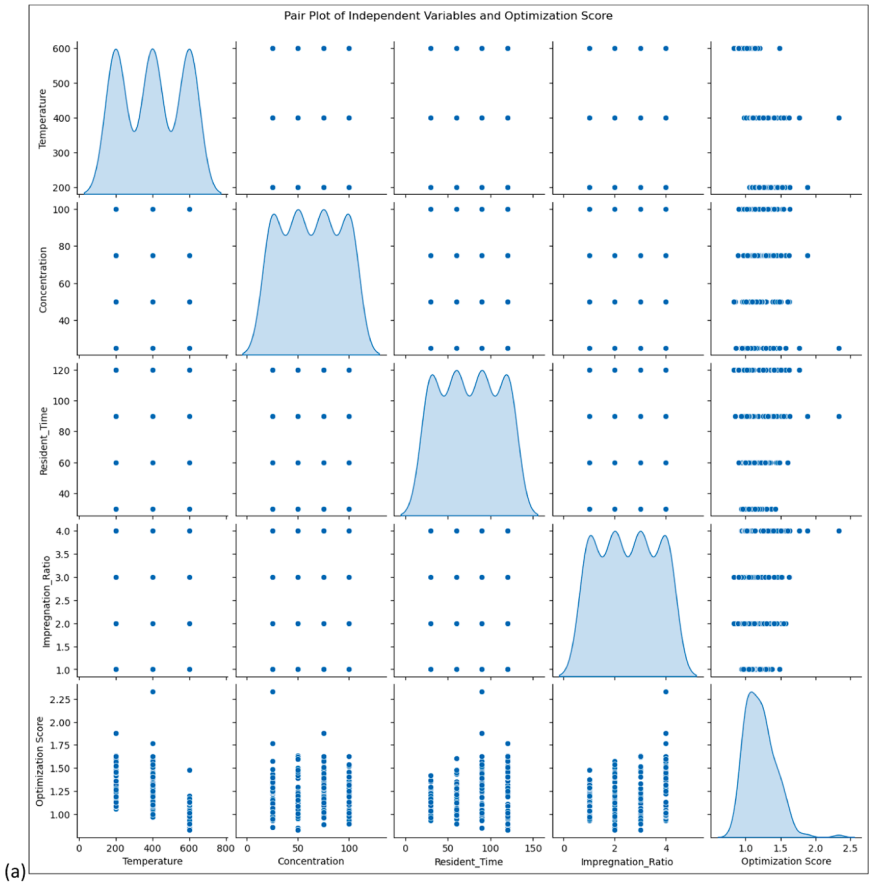

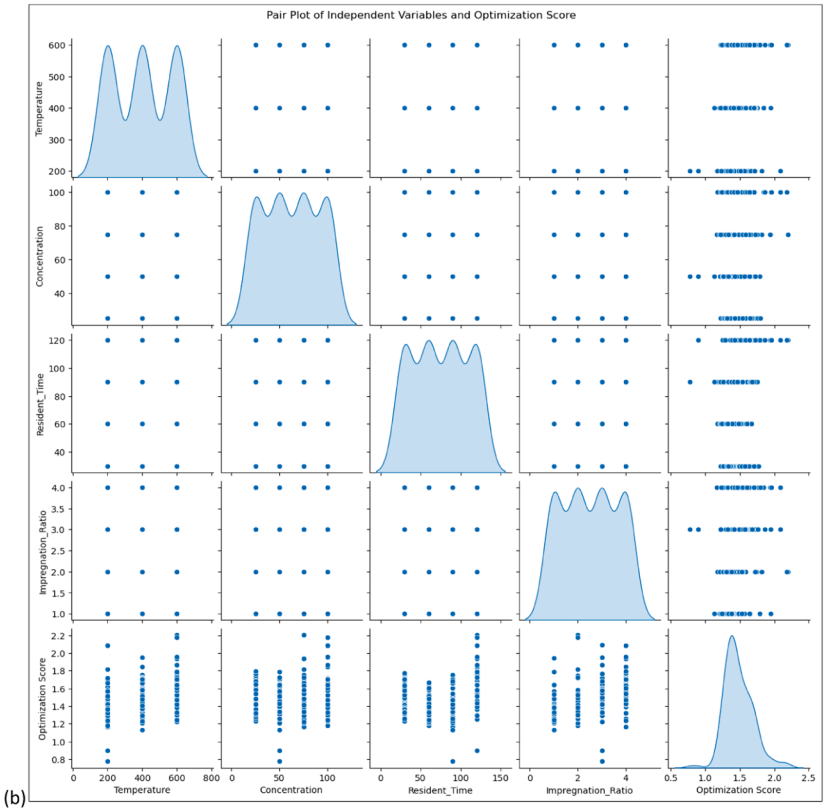

Fig. 11. Pair Plot of input variables and optimization scores for (a) H_3PO_4, (b) $CaCl_2$.

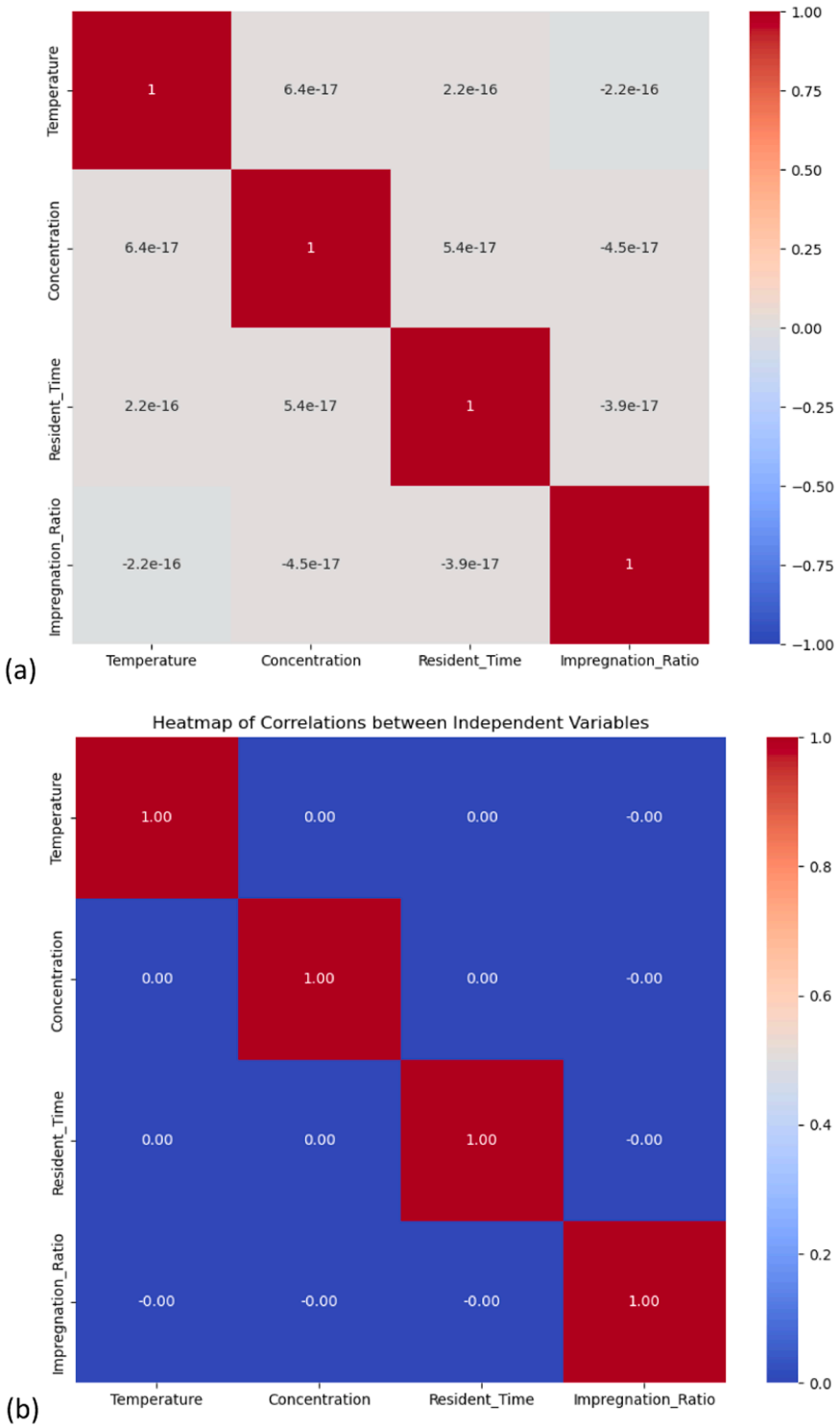

Fig. 12. Correlation between the input variables for (a) H_3PO_4, (b) $CaCl_2$.

The response variation concerning residence time appears minimal, indicating that ash content remains relatively constant regardless of the concentration. Similarly, Fig. 15c shows that the interaction between residence time and H_3PO_4 concentration exhibits no significant variation, confirming the statistical insignificance of concentration or its interaction with residence time on RNEAC's ash content.

Fig. 16a illustrates the impact of the impregnation ratio on carbon yield for H_3PO_4 across various temperatures, showing a consistent trend with minor fluctuations. The highest carbon yield was achieved at 200 °C with a 2 g/mL impregnation ratio, while the lowest yield occurred at 600 °C with a 3 g/mL ratio. Lower temperatures and moderate impregnation ratios were generally more favourable for higher carbon yield, likely due to the activating agent's efficient removal of inorganic content to enhance the carbon yield of RNEAC. Fig. 16b shows the effect of impregnation ratio and activating agent concentration on carbon yield. The highest yield was recorded at 75 % concentration with a 2 g/ml ratio, while the lowest occurred at 50 % concentration with a 4 g/ml ratio, indicating that both parameters significantly influence carbon yield. Fig. 16c explores the impact of the impregnation ratio on carbon yield across different residence times in the furnace. While residence

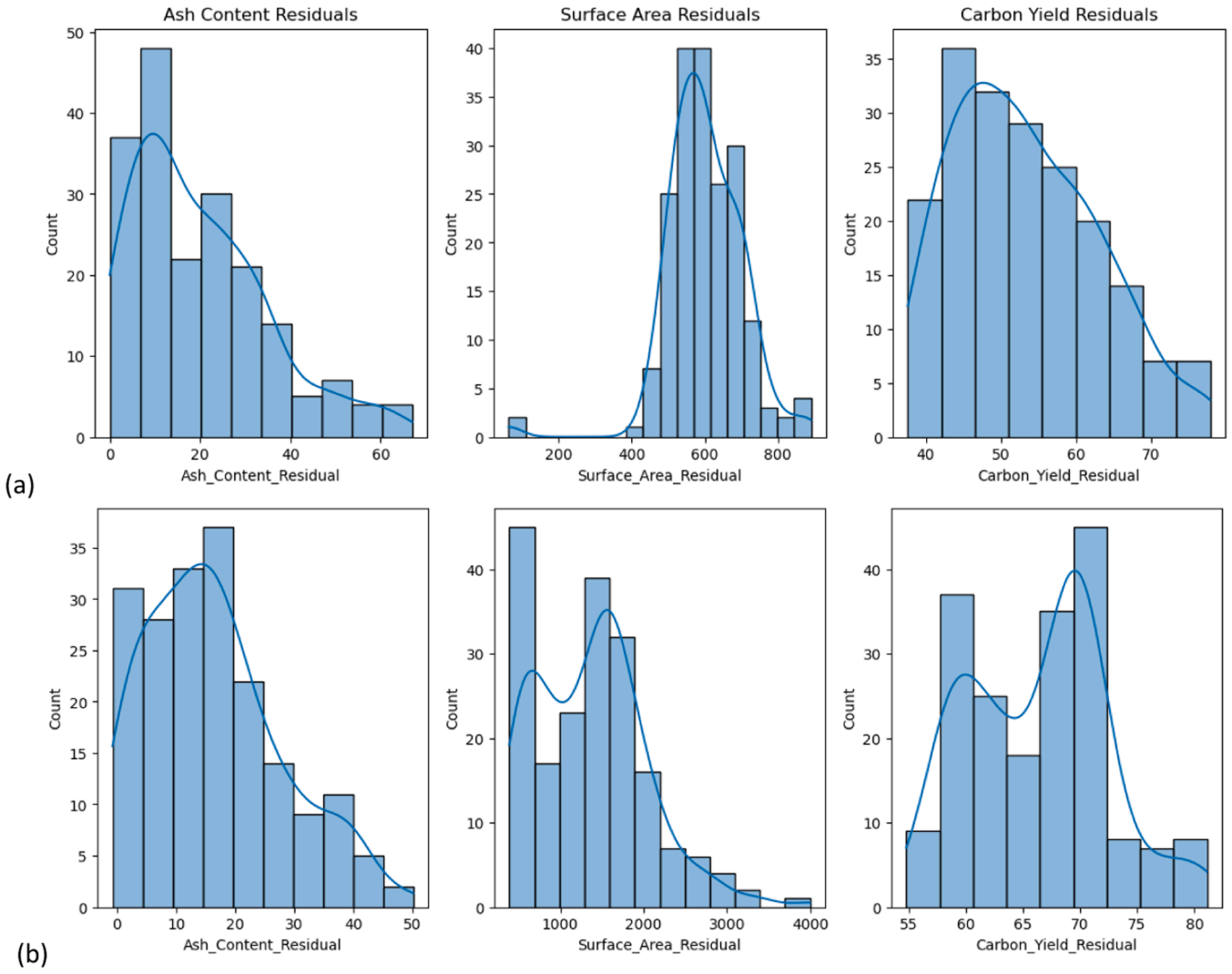

Fig. 13. Histogram of the residuals distribution of dependent variables (a) $CaCl_2$ (b) H_3PO_4.

Table 9
ML Optimal condition for the preparation of RNEAC.

	Group Optimal Condition	
Parameters	$CaCl_2$ value	H_3PO_4 value
Impregnation Ratio (-)	2	4
Temperature (°C)	600	400
Residence Time (mins)	120	90
Concentration (%)	75	25
Ash Content (%)	1	0.22
Carbon Yield (%)	49.9	72
Surface Area (m^2/g)	508.51	1818.2
Optimization Score	2.2	2.33

Table 10
Error analysis result for the experimental data.

Error Indices	Scores	Error Indices	Scores
MAE - Ash Content	1.630	MSE - Ash Content	3.969
MAE - Surface Area	1361.75	MSE - Surface Area	2.29240
MAE - Carbon Yield	66.36	MSE - Carbon Yield	4439.93
Cross-Validation MSE	0.0381 ± 0.00814		
STD of Optimization Score	0.22		
Variance of Optimization Score	0.047		

time influenced carbon yield, its effect diminished at prolonged durations, such as 120 min, likely due to the collapse of the delicate carbon matrix. The highest yield was achieved with a 2 g/ml ratio at a residence time of 90 min, which aligns with the experimental optimal conditions. Fig. 16d illustrates the effect of the impregnation ratio on surface area across various residence times. The surface area shows a minimal increase with higher impregnation ratios at 30, 60, and 120-minute residence times. However, at a 90-minute residence time, an impregnation ratio of 4 g/ml significantly enhances the surface area, demonstrating a positive correlation between impregnation ratio and surface area at this specific duration. This finding aligns with Kwaghger et al. [8], who observed similar trends in mango kernel-activated carbon activated with HCl, where activating agent concentration, impregnation ratios, and residence times collectively influenced the specific surface area of AC materials.

In summary, the influence of H_3PO_4 as an activator on the ash content, surface area, and carbon yield of RNEAC was statistically analyzed. The ANOVA results for ash content indicate that temperature is highly significant, with a p-value of 0. The interaction between temperature and time was also statistically significant, demonstrating a combined effect on ash content. These findings highlight the critical role of temperature and its interaction with time in optimizing the production of RNEAC with H_3PO_4. Such insights are crucial for improving the quality of RNEAC and tailoring its properties for engineering applications, such as in SARs. The study also examined the impact of H_3PO_4 on the surface

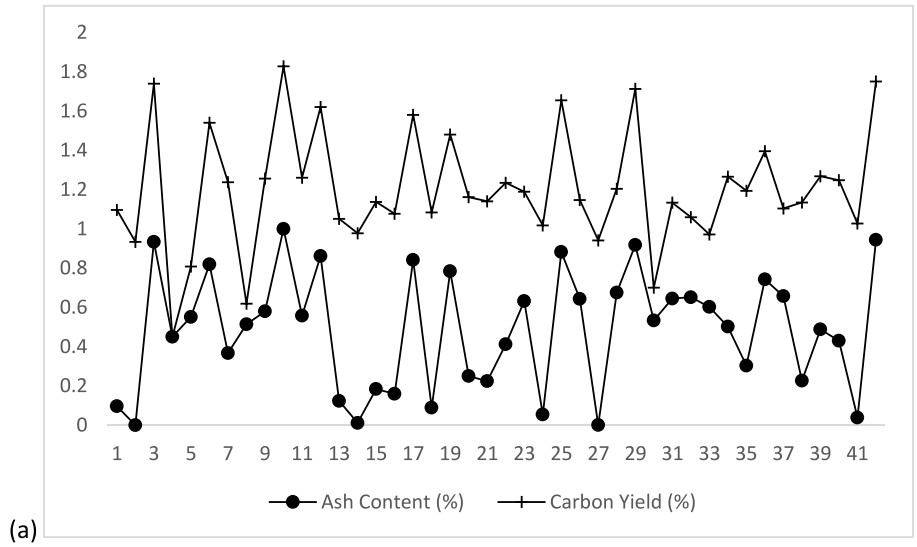

(a)

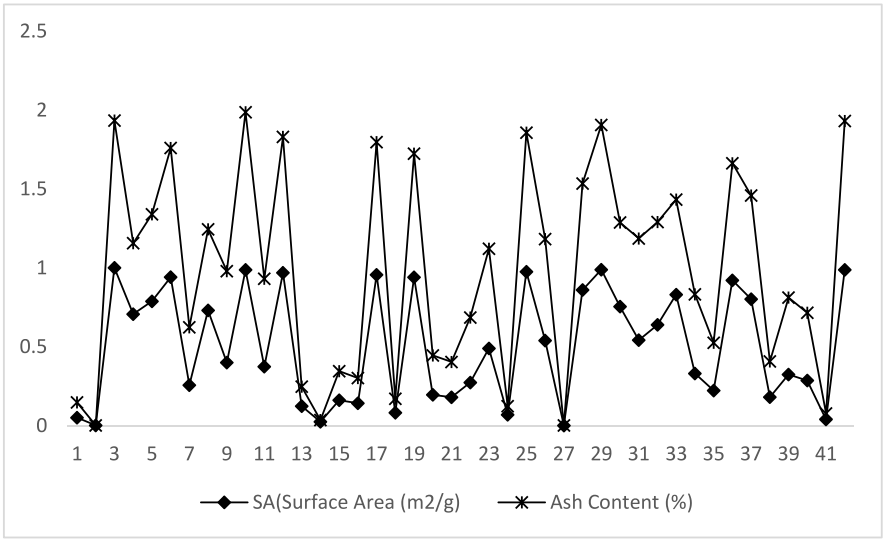

(b)

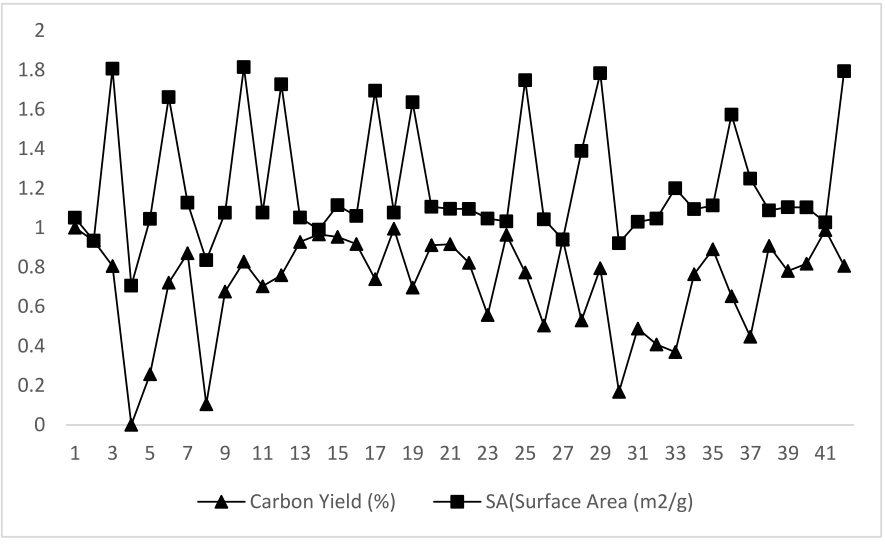

(c)

Fig. 14. Pareto Frontier for trade-offs between parameters (a) ASH Content and Carbon Yield, (b) Ash Content and Surface Area, (c) Surface Area and Carbon Yield.

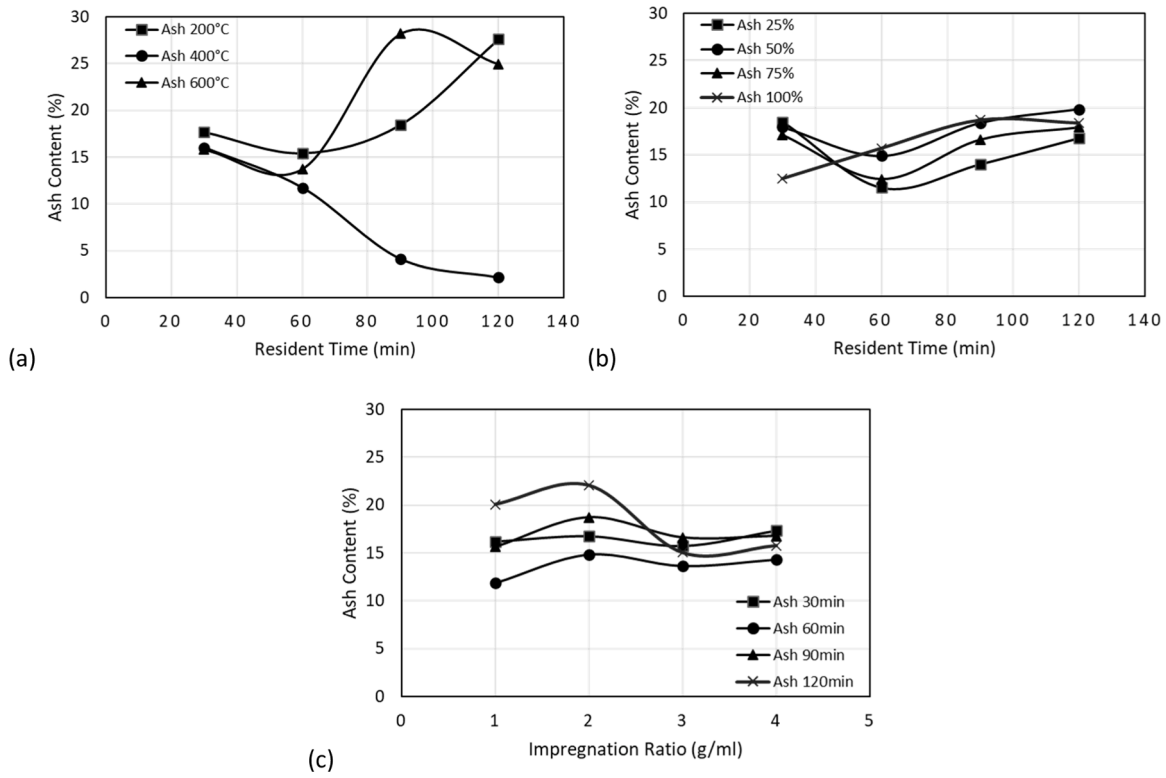

Fig. 15. An interaction effect on ash content (a) residence time and temperature (b) residence time and H_3PO_4 concentration (c) Impregnation ratio and residence time.

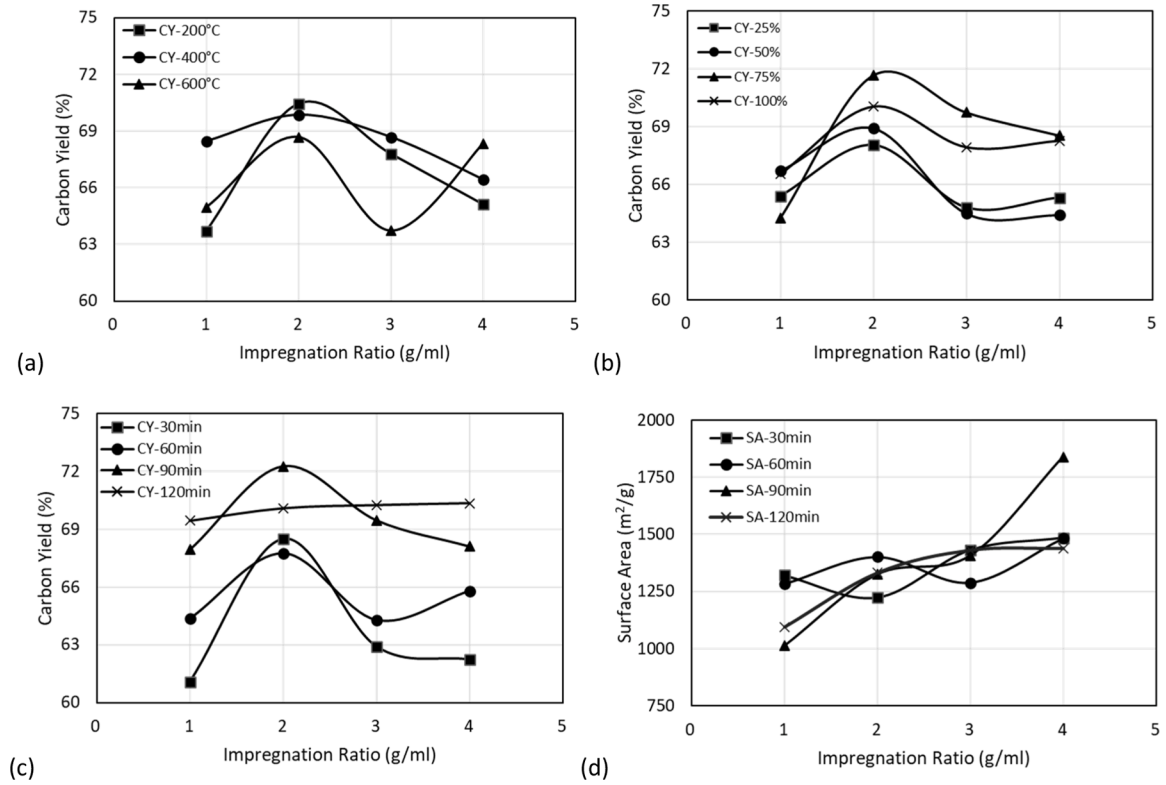

Fig. 16. Interaction effect of impregnation ratio and other process parameters (a) Carbonization temperature on carbon yield (b) H_3PO_4 Concentration on carbon yield (c) Resident time on carbon yield (d) Resident time on surface area of RNEAC.

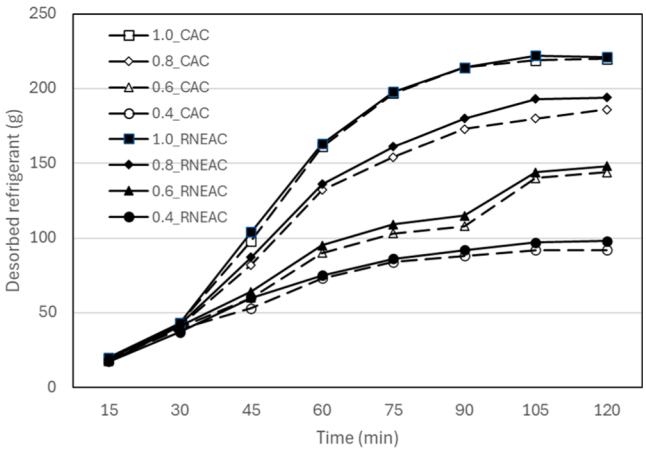

Fig. 17. Adsorption/Desorption Patterns of Desorbed Refrigerant for RNEAC and CAC.

area of RNEAC. Significant factors influencing surface area included impregnation ratio, temperature, and their interactions with time, showing p-values below 0.05. These results highlight the importance of these variables in optimizing the pore structure of RNEAC, providing valuable guidance for enhancing its adsorption capabilities through precise control of activation conditions. Furthermore, the effect of H_3PO_4 on the carbon yield of RNEAC was evaluated, revealing statistically significant influences from impregnation ratio, activation time, concentration, and their interactions (cf. Appendix 3). The interactions of ratio with time and temperature with time were particularly noteworthy. These findings underscore the combined effects of these parameters in maximizing carbon yield and optimizing the activation process.

3.6. Validation of RNEAC effectiveness

To test the effectiveness of the optimized RNEAC, Sorption kinetics and capacity retention studies were conducted using a purpose-built solid adsorption refrigeration test rig [25]. The changes in adsorption and desorption rates with cycles were tested and benchmarked against the well-known commercial activated carbon (CAC). Technically, the adsorption/desorption characteristics of the adsorbent-adsorbate interaction in a SAR system depend on the type of activated carbon used. As such, 500 g of RNEAC and CAC each was evaluated with varying masses of methanol (as refrigerant) in the range of 0.4, 0.6, 0.8 and 1.0 g for 120 min at a 15-minute time step. Fig. 17 shows the refrigerant's desorption patterns over time for RNEAC and GAC adsorbents. The result is consistent with theoretical expectations, as an increase in the adsorbent's initial resident time proportionately correlates with the refrigerant desorbed. The curve exhibits a plateau between 105 and 120 min, signifying a transition towards saturation. Additionally, the RNEAC's desorption and adsorption capacity compared favourably with the CAC and even slightly outperformed the CAC. This is interesting and reveals the apparent potential of RNEAC, considering the refinement it can still undergo over time compared to the commercially available AC that's already matured.

4. Conclusion and recommendations

This study demonstrates the successful transformation of Raphia nut endocarp (RNE) into high-performance activated carbon (RNEAC) using calcium chloride ($CaCl_2$) and phosphoric acid (H_3PO_4) as activating agents. The production process was comprehensively optimized by integrating genetic algorithms, Pareto optimality, min-max normalization, and machine learning to achieve desirable adsorbent characteristics, including low ash content, high surface area, and superior carbon yield. Quantitative pore structure assessment using Scanning Electron Microscopy (SEM) coupled with ImageJ analysis confirmed the presence of a well-developed porous network, validating the effectiveness of the activation strategy. The experimental validation revealed that the optimized RNEAC matched and slightly outperformed commercial activated carbon in terms of adsorption capacity within the solid adsorption refrigeration (SAR) test rig. This is particularly significant as it demonstrates that agro-waste can be converted into high-performance adsorbents suitable for environmentally friendly, off-grid cooling solutions. These findings further highlight the potential of agricultural waste valorization in addressing cooling and environmental challenges, particularly in resource-constrained communities. Collectively, this dual benefit will advance the development of scalable, environmentally sustainable cooling technologies for rural and off-grid areas.

Future work should focus on refining the pore size distribution and enhancing surface chemistry to improve adsorption kinetics for natural refrigerants. Exploring alternative low-cost activating agents, optimizing physical form factors, and conducting lifecycle assessments will further support commercial scalability. Combining computational modelling with experimental validation can also streamline the development of next-generation sustainable adsorbents tailored for application in SARs. The practical considerations for the real-world deployment of this technology in off-grid communities are essential for the economic viability and scalability of the manufacturing process. Additionally, further study should consider long-term durability testing of RNEAC in a real SAR system to evaluate its mechanical and thermal stability.

Data availability

Data will be made available on request.

CRediT authorship contribution statement

Rasheed B. Ayoola: Writing – original draft, Software, Methodology, Investigation, Formal analysis, Data curation. **Olusegun M. Ilori:** Writing – review & editing, Supervision, Project administration, Methodology, Funding acquisition. **Sikiru A. Amidu:** Writing – review & editing, Supervision, Project administration, Methodology. **Maryam T. Buhari:** Writing – review & editing, Project administration. **Moruf O. Yusuf:** Writing – review & editing, Supervision, Software, Methodology. **Alex O. Edeoja:** Writing – review & editing, Supervision, Project administration, Investigation. **Jacob S. Ibrahim:** Writing – review & editing, Supervision, Software, Methodology.

Declaration of competing interest

The authors declare that they have no known competing financial interests or personal relationships that could have appeared to influence the work reported in this paper.

Acknowledgement

The authors are grateful for the PhD funding support provided by the Faculty of Computing, Engineering and the Built Environment (now School of Architecture, Built Environment, Computing, and Engineringg), Birmingham City University, through the Faculty Dean Scholarship Award.

Appendix 1. RNEAC Production Parameters Optimization with Genetic Algorithm (Pareto Optimal Front)

Ratio	Temp.	Time	Conc.	Ash Content (%)	Carbon Yield (%)	Surface Area (m^2/g)
1.6989	399.98	116.11	95.587	3.3099	73.753	1440.6
2.2972	400.06	109.72	75.392	1.0447	73.15	1402.3
3.9797	208.41	119.99	96.614	22.942	71.984	2176.6
2.7982	211.78	66.706	34.846	11.602	64.636	1948.9
3.2299	219.56	79.965	54.763	13.981	66.978	2011.9
3.5822	230.67	117.21	89.124	20.256	71.211	2130.7
3.514	370.46	117.9	93.852	9.6582	72.571	1600.1
2.6798	220.73	73.313	41.843	13.094	65.591	1967.5
2.9866	348.59	117.26	93.418	14.647	70.801	1710.9
3.9708	210.03	119.98	85.813	24.505	72.18	2166.3
2.7374	351.61	117.05	90.836	14.127	71.045	1690.8
3.8253	223.48	119.25	93.603	21.259	71.558	2151.9
2.6127	384.18	114.41	79.268	3.9421	73.094	1497.1
2.4261	398.51	114.39	79.638	1.3064	73.446	1419.9
2.5144	383.1	116.86	91.41	5.3617	73.326	1526.2
3.296	381.8	115.75	79.279	4.7858	73	1511.5
2.8704	221.26	112.59	95.576	20.785	71.374	2141.9
1.7948	394.75	116.08	93.093	3.1282	73.706	1464.8
3.2787	234.76	119.58	92.163	19.437	70.985	2129.8
2.6758	376.88	115.94	87.655	6.9111	72.944	1552.6
2.4774	378.37	117.1	85.207	6.2983	72.99	1540.6
2.6936	365.32	114.5	87.853	10.714	72.132	1613
3.5523	334.8	117.44	94.311	15.867	69.716	1780.5
2.4023	392.57	118.58	80.268	2.3123	73.422	1454.8
3.8868	220.51	119.38	93.961	21.737	71.684	2157.2
3.9061	327.55	119.26	95.808	16.133	69.228	1819.3
2.416	400.38	111	75.737	1.0573	73.211	1401.7
2.9788	259.25	119.13	90.497	16.876	69.463	2067.6
3.56	214.28	119.86	95.268	22.577	71.883	2167.6
3.2086	220.2	77.694	43.899	13.549	66.161	1986
3.1891	325.17	118.61	91.095	16.172	69.09	1821.1
3.2114	306.72	116.55	89.452	16.33	68.354	1896.3
2.58	212.66	83.763	63.193	15.171	68.003	2045.1
2.8497	358.2	114.85	91.931	12.82	71.601	1657.4
3.4528	373.6	116.44	88.961	8.16	72.753	1573.7
3.4185	241.28	119.34	91.46	18.467	70.586	2115
2.8176	273.95	118.54	91.352	16.457	68.711	2022.9
3.1445	377.77	116.31	83.465	6.3587	72.911	1541
3.5035	359.96	117.34	92.526	12.486	71.75	1652.4
2.9294	364.44	117.25	89.337	11.13	72.092	1622.6
3.0024	398.85	116.64	86.206	1.945	73.649	1431.5
3.8751	212.94	119.3	92.381	23.183	71.99	2166.6

Appendix 2. Result of Pareto Optimization from Multi-objective Genetic Algorithm (MOGA) and Min-Max Normalisation

Ranked Scenarios	Scenarios	Ratio	Temp	Time	Conc	Ash Content (%)	Carbon Yield (%)	Surface Area (m2/g)	Composite Score
1	26	2.416	400.38	111	75.737	1.0573	73.211	1401.7	0.000269
2	1	2.2972	400.2	109.72	75.392	1.0447	73.15	1402.3	0.000387
3	13	2.4261	398.51	114.39	79.638	1.3064	73.446	1419.9	0.017321

(*continued on next page*)

(*continued*)

Ranked Scenarios	Scenarios	Ratio	Temp	Time	Conc	Ash Content (%)	Carbon Yield (%)	Surface Area (m2/g)	Composite Score
4	40	3.0024	398.85	116.64	86.206	1.945	73.649	1431.5	0.038416
5	23	2.4023	392.57	118.58	80.268	2.3123	73.422	1454.8	0.061278
6	0	1.6989	399.98	116.11	95.587	3.3099	73.753	1440.6	0.073377
7	17	1.7948	394.75	116.08	93.093	3.1282	73.706	1464.8	0.08512
8	12	2.6127	384.18	114.41	79.268	3.9421	73.094	1497.1	0.123307
9	15	3.296	381.8	115.75	79.279	4.7858	73	1511.5	0.15058
10	14	2.5144	383.1	116.86	91.41	5.3617	73.326	1526.2	0.172339
11	20	2.4774	378.37	117.1	85.207	6.2983	72.99	1540.6	0.201592
12	37	3.1445	377.77	116.31	83.465	6.3587	72.911	1541	0.203138
13	19	2.6758	376.88	115.94	87.655	6.9111	72.944	1552.6	0.222396
14	34	3.4528	373.6	116.44	88.961	8.16	72.753	1573.7	0.262628
15	6	3.514	370.46	117.9	93.852	9.6582	72.571	1600.1	0.311593
16	21	2.6936	365.32	114.5	87.853	10.714	72.132	1613	0.342418
17	39	2.9294	364.44	117.25	89.337	11.13	72.092	1622.6	0.357478
18	38	3.5035	359.96	117.34	92.526	12.486	71.75	1652.4	0.405607
19	33	2.8497	358.2	114.85	91.931	12.82	71.601	1657.4	0.415951
20	10	2.7374	351.61	117.05	90.836	14.127	71.045	1690.8	0.465358
21	8	2.9866	348.59	117.26	93.418	14.647	70.801	1710.9	0.48941
22	22	3.5523	334.8	117.44	94.311	15.867	69.716	1780.5	0.56032
23	3	2.7982	211.78	66.706	34.846	11.602	64.636	1948.9	0.578081
24	25	3.9061	327.55	119.26	95.808	16.133	69.228	1819.3	0.591025
25	30	3.1891	325.17	118.61	91.095	16.172	69.09	1821.1	0.593018
26	7	2.6798	220.73	73.313	41.843	13.094	65.591	1967.5	0.621881
27	29	3.2086	220.2	77.694	43.899	13.549	66.161	1986	0.643516
28	31	3.2114	306.72	116.55	89.452	16.33	68.354	1896.3	0.644907
29	4	3.2299	219.56	79.965	54.763	13.981	66.978	2011.9	0.669434
30	32	2.58	212.66	83.763	63.193	15.171	68.003	2045.1	0.716219
31	36	2.8176	273.95	118.54	91.352	16.457	68.711	2022.9	0.729302
32	27	2.9788	259.25	119.13	90.497	16.876	69.463	2067.6	0.767075
33	35	3.4185	241.28	119.34	91.46	18.467	70.586	2115	0.831567
34	18	3.2787	234.76	119.58	92.163	19.437	70.985	2129.8	0.86179
35	5	3.5822	230.67	117.21	89.124	20.256	71.211	2130.7	0.879826
36	16	2.8704	221.26	112.59	95.576	20.785	71.374	2141.9	0.898327
37	11	3.8253	223.48	119.25	93.603	21.259	71.558	2151.9	0.914882
38	24	3.8868	220.51	119.38	93.961	21.737	71.684	2157.2	0.928489
39	28	3.56	214.28	119.86	95.268	22.577	71.883	2167.6	0.953102
40	41	3.8751	212.94	119.3	92.381	23.183	71.99	2166.6	0.965372
41	2	3.9797	208.41	119.99	96.614	22.942	71.984	2176.6	0.966688
42	9	3.9708	210.03	119.98	85.813	24.505	72.18	2166.3	0.993354

Appendix 3. Response Optimization Solutions

Ranking order	T °C	Conc (%)	RT (min)	IR (g/g)	CY (%)	SA (m^2/g) Fit	AS-C (%) Fit	Composite Desirability
1	212.121	100	120	4	74.7738	2755	12.4565	0.710484
2	249.955	100	119.699	3.77491	75.3321	2443.33	10.7079	0.694713
3	206.711	58.182	120	3.69579	71.8448	2574.02	18.9947	0.614683
4	282.464	98.895	117.76	2.50949	75.8463	1826.89	14.2238	0.603103
5	278.461	48.873	120	3.75534	70.9711	2166.6	13.3352	0.595655
6	436.331	100	95.315	3.40906	72.7223	1369.98	7.2812	0.532775
7	298.499	26.127	120	1.82128	70.765	1542.14	12.2763	0.518273
8	349.774	95.465	71.731	2.06976	70.383	1455.13	8.4617	0.51693
9	348.37	35.116	64.022	3.11654	67.3442	1558.14	9.3927	0.490333
10	423.798	29.966	112.541	3.90631	67.4382	1345.05	9.253	0.460291
11	336.647	25.178	54.909	1.40683	66.454	1364.7	6.638	0.459735
12	460.386	100	34.667	3.81677	65.8485	1322.73	6.352	0.445535
13	447.129	41.526	68.509	1	67.1074	1156.66	5.5402	0.436331
14	417.462	90.522	93.515	1.12914	69.9505	1084.09	11.8516	0.431583
15	425.582	29.414	33.939	1.4603	65.7893	1230.46	5.9079	0.430992
16	433.58	88.497	33.056	1.48658	65.3682	1211.14	8.5372	0.413248
17	411.368	34.098	33.571	3.29833	64.9351	1298.26	10.9286	0.412787

Note: T °*C* = Temperature, Conc (%) = Concentration, RT (min), IR = Impregnation_Ratio, CY (%) = Carbon_Yield, AS-C (%) = Ash_Content, SA (m^2/g) = Surface_Area

Appendix 4. ANOVA for the Effect of H_3PO_4 on ash content of the RNEAC

The alpha value is 0.05 (95 % confidence level).

Source	Sum Sq.	d.f.	Mean Sq.	F	Prob>F
Ratio	216.51	3	72.17	1.04	0.3787
Temp	5941.73	2	2970.86	42.66	0
Time	527.15	3	175.72	2.52	0.0604
Conc	164.94	3	54.98	0.79	0.5017
Ratio*Temp	874.84	6	145.81	2.09	0.0579
Ratio*Time	350	9	38.89	0.56	0.8289
Ratio*Conc	1091.31	9	121.26	1.74	0.0855
Temp*Time	5260.3	6	879.72	12.59	0
Temp*Conc	829.78	6	138.30	1.99	0.0719
Time*Conc	471.37	9	52.37	0.75	0.6606
Error	9401.07	135	69.64		
Total	25,128.98	191			

Appendix 5. ANOVA for the Effect of H_3PO_4 on surface area of the RNEAC

Source	Sum Sq.	d.f.	Mean Sq.	F	Prob>F
Ratio	4345,238	3	1448,412.7	19.61	0
Temp	53,769,095.9	2	26,884,548	363.92	0
Time	41,742.4	3	13,914.1	0.19	0.9042
Conc	428,225.4	3	142,741.8	1.93	0.1273
Ratio*Temp	10,326,021.8	6	1721,003.6	23.3	0
Ratio*Time	2119,652.7	9	235,517	3.19	0.0016
Ratio*Conc	1016,015	9	112,890.6	1.53	0.144
Temp*Time	3524,255.9	6	587,376	7.95	0
Temp*Conc	444,854.3	6	74,142.4	1	0.4257
Time*Conc	370,128.1	9	41,125.3	0.56	0.8303
Error	9973,094.5	135	73,874.8		
Total	86,358,323.8	191			

Appendix 6. ANOVA for the Effect of the Activating Agents on Carbon Yield of the RNEAC

Source	Sum Sq.	d.f.	Mean Sq.	F	Prob>F
Ratio	422.72	3	140.907	6.33	0.0005
Temp	135.48	2	67.738	3.04	0.0509
Time	1352.13	3	450.711	20.25	0
Conc	273.05	3	91.018	4.09	0.0081
Ratio*Temp	388.49	6	64.748	2.91	0.0106
Ratio*Time	215.45	9	23.939	1.08	0.3846
Ratio*Conc	249.19	9	27.688	1.24	0.2734
Temp*Time	632.08	6	105.347	4.73	0.0002
Temp*Conc	274.23	6	45.706	2.05	0.0627
Time*Conc	161.25	9	17.916	0.81	0.6122
Error	3004.06	135	22.252		
Total	7108.11	191			

References

[1] M. Crippa, E. Solazzo, D. Guizzardi, F. Monforti-Ferrario, F.N. Tubiello, A.J.N. F. Leip, Food systems are responsible for a third of global anthropogenic GHG emissions, Nat. Food 2 (3) (2021) 198–209.

[2] H.M. Khan, T. Iqbal, S. Yasin, C.H. Ali, M.M. Abbas, M.A. Jamil, A. Hussain, M. Soudagar, M. E, M.M. Rahman, Application of agricultural waste as heterogeneous catalysts for biodiesel production, Catalysts. 11 (10) (2021) 1215.

[3] F.N. Tubiello, M. Salvatore, S. Rossi, A. Ferrara, N. Fitton, P. Smith, The FAOSTAT database of greenhouse gas emissions from agriculture, Environ. Res. Lett. 8 (1) (2013) 015009.

[4] United Nations Environment Programme. Division of Early Warning, UNEP Yearbook 2021: Emerging Issues in Our Global Environment, UNEP/Earthprint, 2021.

[5] Missing Food : The Case of Postharvest Grain Losses in Sub-Saharan, Africa, 2011.

[6] F.S. Baker, C.E. Miller, A.J. Repik, E.D. Tolles, Activated carbon, Kirk-Othmer Encyclopedia of Chem. Technol. (2000), https://doi.org/10.1002/0471238961.0103200902011105.a01.

[7] O.S. Bello, E.S. Owojuyigbe, M.A. Babatunde, Sustainable conversion of agro-wastes into useful adsorbents, Appl. Water. Sci. 7 (2017) 3561–3571, https://doi.org/10.1007/s13201-016-0494-0.

[8] A.K. Kwaghger, J.S. Ibrahim, A.O. Edeoja, R.B. Ayoola, Evaluation of activated carbon from Raphia palm nut endocarp as adsorbent for solid adsorption refrigeration, J. Eng. Res. Reports (2022) 24–47.

[9] F. Miksík, T. Miyazaki, K. Thu, J. Miyawaki, K. Nakabayashi, A.T. Wijayanta, F. Rahmawati, Enhancing water adsorption capacity of acorn nutshell based activated carbon for adsorption thermal energy storage application, Energy Reports 6 (2020) 255–263, https://doi.org/10.1016/j.egyr.2020.11.038.

[10] L. Kitinoja, Use of Cold Chains For Reducing Food Losses in Developing Countries, Purdue University, 2013.

[11] S. Singh, Preservation technologies for fresh fruits and vegetables, Stewart Postharvest Review 7 (1) (2011) 1–7.

[12] O.M. Ilori, A.J. Jaworski, X. Mao, Experimental and numerical investigations of thermal characteristics of heat exchangers in oscillatory flow, App. Ther. Eng. 144 (2018) 910–925.

[13] G.D. Akpen, I.L. Nwaogazie, T.G. Leton, Optimum conditions for the removal of color from wastewater by mango seed shell-based activated carbon, Indian J. Sci. Technol. 4 (8) (2011) 890–894, https://doi.org/10.17485/ijst/2011/v4i8.16.

[14] H. Demir, M. Mobedi, S. Ülkü, A review on adsorption heat pump: problems and solutions, Renew. Sustain. Energy Rev. 9 (2008) 2381–2403.

[15] Mahmoud B. Elsheniti, O.A. Elsamni, S. Mahmoud, E. Elsayed, K. Saleh, Adsorption Refrigeration Technologies. Sustain. Air Cond. Syst., 2018, https://doi.org/10.5772/intechopen.73167.

[16] M. Luberti, C. Di Santis, G. Santori, Ammonia/ethanol mixture for adsorption refrigeration, Energies. (Basel) 13 (4) (2020) 983, https://doi.org/10.3390/en13040983, online.

[17] E.R. Raut, M.A.B. Thakur, A.R. Chaudhari, A review on activated carbon preparation from natural and eco-friendly raw materials, in: AIP Conference Proceedings 2417, AIP Publishing, 2021.

[18] J.A. Watson, D. Treadwell, S.A. Sargent, J.K. Brecht, W. Pelletier, Postharvest storage, Packaging and Handling of Speciality crops: a Guide For Florida small Farm Producers, IFAS Extension the University of Florida, 2015.

[19] E.E. Anyanwu, C.I. Ezekwe, Design, construction and test run of a solid adsorption solar refrigerator using activated carbon/methanol as adsorbent/adsorbate pair, Energy Con. Manag. 44 (18) (2003) 2879–2892.

[20] L.W. Wang, R.Z. Wang, R.G. Oliveira, A review on adsorption working pairs for refrigeration, Renew. Sustain. Energy Rev. 13 (3) (2009) 518–534, https://doi.org/10.1016/j.rser.2007.12.002.

[21] M.A. Yahya, Z. Al-Qodah, C.W.Z. Ngah, Agricultural bio-waste materials as potential sustainable precursors used for activated carbon production: A review, Ren. Sustain. Energy Rev. 46 (2015) 218–235.

[22] J. Fu, Q. Kang, W. Ao, et al., Comparison and analysis of one- and two-step activation for preparation of activated carbon from furfural residues, Biomass Conv. Bioref. 13 (2023) 4681–4694, https://doi.org/10.1007/s13399-021-01439-4.

[23] M.S. Reza, C.S. Yun, S. Afroze, et al., Preparation of activated carbon from biomass and its' applications in water and gas purification, a review, Arab. J. Basic Appl. Sci. 27 (1) (2020) 208–238, https://doi.org/10.1080/25765299.2020.1766799.

[24] S.M. Yakout, G.S. El-Deen, Characterization of activated carbon prepared by phosphoric acid activation of olive stones, Arab. J. Chem. 9 (2016) S1155–S1162.

[25] R.B. Ayoola, A.O. Edeoja, J.S. Ibrahim, A.K. Kwaghger, Evaluation of activated carbon from Raphia palm nut endocarp as adsorbent for solid adsorption refrigeration, System 43 (2022) 46, https://doi.org/10.9734/JERR/2022/v23i10750.

[26] S.M. Kamga, B. Sonké, T.L. Couvreur, Raphia vinifera (Arecaceae; Calamoideae): misidentified for far too long, Biodivers Data J. 7 (2019).

[27] R.Z. Wang, R.G. Oliveira, Adsorption refrigeration—An efficient way to make good use of waste heat and solar energy, Prog. Energy Combust. Sci. 32 (4) (2006) 424–458.

[28] P. Boruta, T. Bujok, Ł. Mika, K. Sztekler, Adsorbents, Working Pairs and Coated Beds for Natural Refrigerants in Adsorption Chillers—State of the Art, Energ. 14 (15) (2021) 4707.

[29] L. Lu, C.M. Anderson-Cook, T.J. Robinson, Optimization of designed experiments based on multiple criteria utilizing a Pareto frontier, Technometrics. 53 (4) (2011) 353–365.

[30] M ⁋⁋Li, RZ Wang, YX Xu, JY Wu, AO Dieng, Experimental ⁋study on dynamic performance analysis of ⁋a ⁋flat–plate solar ⁋solid–adsorption refrigeration for ice maker, Ren. Energy ⁋⁋ 27 (2) (2002) 211–221.

[31] N. Abuelnoor, A. AlHajaj, M. Khaleel, L.F. Vega, M.R. Abu-Zahra, Activated carbons from biomass-based sources for CO2 capture applications, Chemosphere 282 (2021) 131111.

[32] M. Fazal-ur-Rehman, Methodological trends in preparation of activated carbon from local sources and their impacts on production: a review, Chem. Int 4 (2018) 109–119.

[33] M.N. Hossain, M.D. Islam, A. Rahaman, N. Khatun, M.A. Matin, Production of cost-effective activated carbon from tea waste for tannery waste water treatment, Appl. Water Sci. 13 (3) (2023) 73.

[34] R. Briones, L. Serrano, R.B. Younes, I. Mondragon, J. Labidi, Polyol production by chemical modification of date seeds, Ind. Crops Prod. 34 (1) (2011) 1035–1040.

[35] K. Hu, Y. Liu, Q. Zhang, Z. Song, M.A. Thaika, R. Li, E. Kuru, J. Shi, H. Liu, From micropores to macropores: investigating pore characteristics of Longmaxi shale in the Sichuan Basin, Energy Fuels 38 (5) (2024) 3961–3981.

[36] Kaldenhoven, R.G. and Hill, J.M., 2018. Determining the pore structure of activated carbon by nitrogen gas adsorption.

[37] C. Chilev, Y. Stoycheva, M. Dicko, F. Lamari, P. Langlois, I. Pentchev, A new procedure for porous material characterization, Int. J. Sci., Technol. Soc. 5 (4) (2017) 131–140.

[38] M.R. Hossen, M.W. Talbot, R. Kennard, D.W. Bousfield, M.D. Mason, A comparative study of methods for porosity determination of cellulose based porous materials, Cellulose 27 (2020) 6849–6860.

[39] M.B. Sweatman, N. Quirke, Characterization of porous materials by gas adsorption: comparison of nitrogen at 77 k and carbon dioxide at 298 k for activated carbon, Langmuir. 17 (16) (2001) 5011–5020.

[40] J. Maheshwaran, J. Jerlin Regin, A. Ilanthalir, D. Maheswaran, Influence of chemical and thermal treatment methods on the mechanical and micro-structural characteristics of coconut shell based concrete, Global NEST J. 25 (10) (2023) 56–64.

[41] O. Agboola, B. Okoli, S.E. Sanni, P.A. Alaba, P. Popoola, E.R. Sadiku, P.M. Mubiayi, E.T. Akinlabi, M.E. Makhatha, Synthesis of activated carbon from olive seeds: investigating the yield, energy efficiency, and dye removal capacity, SN. Appl. Sci. 1 (2019) 1–10.

[42] Z. Hu, M.P. Srinivasan, Preparation of high-surface-area activated carbons from coconut shell. Microporous and Mesoporous, Mat. 27 (1) (1999) 11–18.

[43] K.Y. Foo, B.H. Hameed, Porous structure and adsorptive properties of pineapple peel-based activated carbons prepared via microwave-assisted KOH and K_2CO_3 activation, Micro. Meso. Mat. 148 (2012) 191–195.

[44] T. Jayalakshmi, A. Santhakumaran, Statistical normalization and backpropagation for classification, Int. J. Comput. Theory Eng. 3 (1) (2011) 1793–8201.

[45] J. Serafin, B. Dziejarski, Activated carbons—Preparation, characterization and their application in CO2 capture: a review, Environ. Sci. Pollut. Res. (2023) 1–55.

[46] H. Boulika, M. El Hajam, M.H. Nabih, N.I. Kandri, A. Zerouale, Activated carbon from almond shells using an eco-compatible method: screening, optimization, characterization, and adsorption performance testing, RSC Adv 12 (53) (2022) 34393–34403.

[47] Alam, T., Qamar, S., Dixit, A. and Benaida, M., 2020. Genetic algorithm: reviews, implementations, and applications. *arXiv preprint arXiv:2007.12673*.

[48] A. Freni, G. Maggio, S. Vasta, G. Santori, F. Polonara, G. Restuccia, Optimization of a solar-powered adsorptive ice-maker by a mathematical method, Solar Energy 82 (11) (2008) 965–976.

[49] S. Verma, M. Pant, V. Snasel, A comprehensive review of NSGA-II for multi-objective combinatorial optimization problems, IEEe Access. 9 (2021) 57757–57791.

[50] Elham Kabiri, Negin Maftouni, Multiple objective energy optimization of a trade center building based on genetic algorithm using ecological materials, Nat. Sci. Reports (14) (2024) 9366, https://doi.org/10.1038/s41598-024-58515-8.

[51] J. Zhang, M. Li, W. Liu, S. Lauria, X. Liu, Many-objective optimization meets recommendation systems: a food recommendation scenario, Neurocomputing. 503 (2022) 109–117.

[52] He, X., Chen, X., Wang, X., Jiang, L. (2023). Optimization of activated carbon production from corn cob using response surface methodology. https://doi.org/10.3389/fenvs.2023.1105408.

[53] N.A. Zolpakar, S.S. Lodhi, S. Pathak, M.A. Sharma, Application of multi-objective genetic algorithm (MOGA) optimization in machining processes, Optimiz. Manuf. Processes (2020) 185–199.

[54] A.D. Mehr, V. Nourani, A Pareto-optimal moving average-multigene genetic programming model for rainfall-runoff modelling, Environ. Modell. Software 92 (2017) 239–251.

[55] W.T. Tsai, T.J. Jiang, Optimization of physical activation process for activated carbon preparation from water caltrop husk, Biomass Conv. Bioref. 13 (2023) 6875–6884, https://doi.org/10.1007/s13399-021-01729-x, 2023.

[56] M. Ehrgott. Multicriteria optimization, 2nd ed., Springer, 2005.

[57] M. Liao, S. Kelley, Y. Yao, Artificial neural network based modeling for the prediction of yield and surface area of activated carbon from biomass, Bio. Bio. Bioref. 13 (4) (2019) 1015–1027.

[58] J. Chang, J.-Y. Lee, Machine learning-based prediction of the adsorption characteristics of biochar from waste wood by chemical activation, Mat. 17 (21) (2024) 5359.

[59] S. Kang, S. Jiang, Z. Peng, Y. Lu, J. Guo, J. Li, W. Zeng, X. Lin, Valorization of humins by phosphoric acid activation for activated carbon production, BioMass Convers. Biorefin. 8 (2018) 889–897.

[60] A.J. Romero-Anaya, A. Molina, P. Garcia, A.A. Ruiz-Colorado, A. Linares-Solano, C. S.M. de Lecea, Phosphoric acid activation of recalcitrant biomass originated in ethanol production from banana plants, Biomass Bioenergy 35 (3) (2011) 1196–1204.

[61] S. Acevedo, L. Giraldo, J.C. Moreno, Caracterización textural y química de carbones activados preparados a partir de cuesco de palma africana (Elaeis guineensis) por activación química con CaCl2 y MgCl2, Revista Colombiana de Química 44 (3) (2015) 18–24.

[62] E. Pehlivan, Production and characterization of activated carbon from pomegranate pulp by phosphoric acid, J. Turkish Chem. Soc. Sect. A: Chem. 5 (1) (2018) 1–8.

[63] I. Pet, M.N. Sanad, M. Farouz, et al., Review: recent developments in the implementation of activated carbon as heavy metal removal management, Water Conserv. Sci. Eng. 9 (2024) 62, https://doi.org/10.1007/s41101-024-00287-3.

[64] Phillip C. Wankat, Lee R. Partin, Process for recovery of solvent vapours with activated carbon, Indust. Eng. Chem. Process Design Dev. 19 (3) (1980) 446–451.

[65] F. Caturla, M. Molina-Sabio, F. Rodriguez-Reinoso, Preparation of activated carbon by chemical activation with ZnCl2, Carbon N Y 29 (7) (1991) 999–1007.

[66] J.A. Beran, Laboratory Manual For Principles of General Chemistry, John Wiley & Sons, 2010.

[67] D.F. Aloko, G.A. Adebayo, Production and characterization of activated carbon from agricultural waste (rice-husk and corn-cob), JEAS-J. Eng. Appl. Sci. 2 (2) (2007) 440–444.

[68] I.A.W. Tan, A.L. Ahmad, B.H. Hameed, Optimization of preparation conditions for activated carbons from coconut husk using response surface methodology, Chem. Eng. J. 137 (3) (2008) 462–470.

[69] K. Deb, A. Pratap, S. Agarwal, T.A.M.T. Meyarivan, A fast and elitist multi-objective genetic algorithm: NSGA-II, IEEE Trans. Evolut. Comput. 6 (2) (2002) 182–197.

[70] H.A. Ahmed, P.J.M. Ali, A.K. Faeq, S.M. Abdullah, An investigation on disparity responds of machine learning algorithms to data normalization method, Aro-The Aci. J. Koya Univ. 10 (2) (2022) 29–37.

[71] A.A. Nasarudin, N. Ngadi, N. Ali, R.A. Rahman, A.N. Sadikin, N.A. Omar, Screening factors influencing adsorption of methylene blue aqueous solution onto immobilized glycerine pitch/sodium alginate beads, in: Third International Conference on Separation Technology 2020 (ICoST 2020), Atlantis Press, 2020, pp. 110–118.

[72] H.P.S. Khalil, M. Jawaid, P. Firoozian, U. Rashid, A. Islam, H.M. Akil, Activated carbon from various agricultural wastes by chemical activation with KOH: preparation and characterization, J. Biobased Mater. Bioenergy 7 (6) (2013) 708–714.

[73] M.L. Martinez, M.M. Torres, C.A. Guzman, D.M. Maestri, Preparation and characteristics of activated carbon from olive stones and walnut shells, Ind. Crops Prod. 23 (1) (2006) 23–28.

[74] H. Demiral, I. Demiral, F. Tümsek, B. Karabacakoğlu, Pore structure of activated carbon prepared from hazelnut bagasse by chemical activation, Surface Interface Anal.: An Int. J. Devot. Dev. Appl. Tech. Anal. Surfaces, Interfaces Thin Films 40 (3–4) (2008) 616–619, 2008.
[75] H.M. Nassar, A. Tekian, A.I. Linjawi, Y.S. Park, Comparative evaluation of weighted mean and composite score for combining assessments, J. Dent. Educ. (2023).
[76] J.W. Wu, S.H. Madani, M.J. Biggs, P. Phillip, C. Lei, E.J. Hu, Characterizations of activated carbon–methanol adsorption pair including the heat of adsorptions, J. Chem. Eng. Data 60 (6) (2015) 1727–1731.
[77] Y. Sun, P.A. Webley, Preparation of activated carbons with large specific surface areas from biomass corncob and their adsorption equilibrium for methane, carbon dioxide, nitrogen, and hydrogen, Ind. Eng. Chem. Res. 50 (15) (2011) 9286–9294.
[78] N. Gunantara, A review of multi-objective optimization: Methods and its applications, Cog. Eng. 5 (1) (2018) 1502242.